To the Graduate Council:

I am submitting herewith a thesis written by Sarah Beth Janney entitled "Blast Resistant Design of Steel Structures." I have examined the final electronic copy of this thesis for form and content and recommend that it be accepted in partial fulfillment of the requirements for the degree of Master of Science, with a major in Civil Engineering.

Qiuhong Zhao
Major Professor

We have read this thesis
and recommend its acceptance:

Edwin G. Burdette

Richard M. Bennett

Accepted for the Council:

Carolyn R. Hodges
Vice Provost and Dean of the
Graduate School

(Original signatures are on file with official student records.)

Blast Resistant Design of Steel Structures

A Thesis Presented for the
Master of Science Degree
The University of Tennessee, Knoxville

Sarah Beth Janney
December 2007

Abstract

The purpose of this study was to examine the load experienced by a steel blast cubicle from a surface blast test. An important objective was to determine the blast load experienced at different standoff distances and the blast resistance capability of the blast cubicle. Three cubicles with standoff distances of 20, 25, and 30ft respectively were simultaneously subjected to a 50lb TNT explosive. The manual *Structures to Resist the Effects of Accidental Explosions, Army TM 5-1300* conservatively predicted the blast pressure loadings obtained from the pressure transducers mounted on the cubicles. Data collected from accelerometers was compared to results from the analysis program SDOF.

The cubicle walls exhibited elastic behavior without any visible permanent deformation. The wall facing the blast was found to experience the greatest loading and was the critical member. The roof, however, experienced substantial deformation. As the standoff distance from the blast increased the pressure loading experienced by the cubicles decreased. The cubicle closest to the blast was likely close to its limit. Thus the structural design of the blast cubicle was efficient and economical without waste of construction material.

Table of Contents

Chapter		Page
Chapter 1	Introduction	10
Chapter 2	Background and Literature Review	12
2.1	Nature of Explosions	12
2.2	Types of Burst	18
2.3	General Considerations for Blast Design	19
2.4	Analysis Techniques	22
2.5	Experimental Work	26
2.6	Design Manuals	28
Chapter 3	Blast Loading	32
3.1	Blast Pressure Parameters	32
3.2	Loadings from a blast	38
3.3	TM 5-1300: External Blast Loading on Structures	44
3.4	Impulsive Blast Loads	62
Chapter 4	Analysis and Results	63
4.1	Introduction	63
4.2	Specimens and Test Setup	64
4.3	Experimental and Theoretical Results	68
4.4	Discussion of Results	89
4.5	Impulsive Blast Load	98
4.6	Summary and Conclusions	100
Chapter 5	Recommendations and Future Work	102
References		104
References		105
Appendix		108
Vita		115

List of Tables

Table Page

Table 3-1 Heat of detonation and heat of combustion 37
Table 3-2 Properties of different explosives 38
Table 3-3 Drag coefficients corresponding to peak dynamic pressure 53
Table 4-1 Pressure-time history values for the front face 69
Table 4-2 Pressure-time history values for the side face 70
Table 4-3 Pressure-time history experimental values for roof 70
Table 4-4 Front face accelerometer results 75
Table 4-5 Wall section free vibration test results 89
Table 4-6 Maximum experimental positive pressure 96
Table 4-7 Stress from blast impulse load 99

List of Figures

Figure Page

Figure 2-1 Variation of overpressure in air with distance at successive time 13
Figure 2-2 Profile for ideal blast wave 15
Figure 2-3 Variation of dynamic pressure with time at a given location..... 16
Figure 2-4 Reflection of a blast wave on ground surface 17
Figure 2-5 Outward motion of the blast wave near the surface in the Mach region 18
Figure 3-1 Idealized pressure-time variation for free air burst 46
Figure 3-2 Front face loading of a rectangular structure 47
Figure 3-3 Velocity of sound in reflected overpressure region versus peak incident overpressure 48
Figure 3-4 Peak dynamic pressure, density of air behind the shock front, and particle velocity versus peak incident pressure..... 49
Figure 3-5 Positive phase shock wave parameters for a hemispherical TNT explosion on the surface 51
Figure 3-6 Negative phase shock wave parameters for a hemispherical TNT explosion on the surface 52
Figure 3-7 Roof and side wall loading 54
Figure 3-8 Peak equivalent uniform roof and side wall pressures 55
Figure 3-9 Scaled rise time of equivalent uniform positive roof and side wall pressures 56
Figure 3-10 Scaled duration of equivalent roof and side wall pressures 57
Figure 3-11 Rear wall loading 59
Figure 4-1 Blast cubicle outside dimensions 65
Figure 4-2 Typical blast cubicle frame and channel construction 65
Figure 4-3 Site Plan 66
Figure 4-4 Locations of PTs and accelerometer 67
Figure 4-5 Dryer Vent Deflection Indicator 67
Figure 4-6 Air Blast Pressure Time History BX-0751 Front Wall 72
Figure 4-7 Air Blast Pressure Time History BX-0751 Side Wall 72
Figure 4-8 Air Blast Pressure Time History BX-0751 Roof 73
Figure 4-9 Acceleration Time History BX-0751 Front Wall..... 76
Figure 4-10 Velocity Time History BX-0751 Front Wall 76
Figure 4-11 Deflection Time History BX-0751 Front Wall 77
Figure 4-12 Air Blast Pressure Time History BX-0752 Front Wall 79
Figure 4-13 Air Blast Pressure Time History BX-0752 Side Wall 79
Figure 4-14 Air Blast Pressure Time History BX-0752 Roof 80
Figure 4-15 Acceleration Time History BX-0752 Front Wall..... 80
Figure 4-16 Velocity Time History BX-0752 Front Wall 81
Figure 4-17 Deflection Time History BX-0752 Front Wall 81
Figure 4-18 Air Blast Pressure Time History BX-0753 Front Wall 83
Figure 4-19 Air Blast Pressure Time History BX-0753 Side Wall 83

Figure 4-20 Air Blast Pressure Time History BX-0753 Roof 84
Figure 4-21 Free Field Surface Burst at 25ft 86
Figure 4-22 Wall section free vibration test setup 88
Figure 4-23 Comparison of front face theoretical and experimental maximum positive pressures 90
Figure 4-24 Comparison of front face theoretical and experimental positive impulses ... 91
Figure 4-25 Comparison of side face theoretical and experimental maximum positive pressures 93
Figure 4-26 Comparison of side face theoretical and experimental positive impulses 94
Figure 4-27 Comparison of front and side face experimental maximum positive pressures 96

List of Symbols

b - decay coefficient

C_D – drag coefficient

C_Dq – drag pressure

C_Dq_o – peak drag pressure

C_E – equivalent load factor

C_r – sound velocity in reflected region

c_o - ambient speed of sound (0.344 m/msec)

E - energy of the explosive charge

F_m – peak external force

H – height of structure

H_{exp}- heat of detonation of explosive in question

H_{TNT}- heat of detonation of TNT

i – unit positive impulse

i^- - unit negative impulse

i_r – unit positive normal reflected impulse

i_r^- - unit negative normal reflected impulse

i_s - positive phase impulse equal to the area under the pressure time curve for P_{so}

K – structural stiffness

L – distance between reflecting surface and free edge in horizontal direction

L_w – wave length of positive pressure phase

M – structural mass

p – pressure

p^- - negative pressure

p_o- ambient pressure (1.014 bar, 14.7 psi)

P_r – peak positive normal reflected pressure

P_r^- - peak negative normal reflected pressure

P_s – positive incident pressure

P_s^- - negative incident pressure

P_{so} – peak positive incident pressure

P_{so}^- - peak negative incident pressure

p(t)- blast pressure with time

q – dynamic pressure

q_o – peak dynamic pressure

R – standoff distance

R_1 – ratio of S/G where G is equal to H or $W_s/2$, whichever is largest

$\overline{R}$ - Sach's scaled distance

S – height of front wall or one-half its width, whichever is smaller

t - time measured from time of arrival of blast wave

t^- - time measured from the start of the negative phase

t_i - intercept on time axis of a triangle with maximum pressure P_{so} having a total area or impulse equal to the impulse of the blast pressure-time curve

t_d – rise time

t_c – clearing time for reflected pressures

t_i' - drag impulse duration

t_o – duration of positive phase of blast pressure

t_o^- - duration of negative phase of blast pressure

t_{of} – fictitious positive phase pressure duration

t_{of}^- - fictitious negative phase pressure duration

t_{rf} – fictitious reflected positive pressure duration

t_{rf}^- - fictitious reflected negative pressure duration

u - peak wind velocity behind the shock front

U – shock front velocity

W – effective charge weight

W_{exp} - weight of the explosive in question

W_s – width of structure

y – displacement

$\ddot{y}$ - acceleration

Z – scaled distance

Chapter 1 : Introduction

Terrorist attacks have brought increased attention to the design of structures to resist explosions. The latest terrorist attacks in the United States include the 1993 World Trade Center (WTC) bombing in New York, the 1995 Murrah Building bombing in Oklahoma City, and most recently the 2001 airplane attacks on the WTC in New York and the Pentagon in Washington, DC. In the 1993 bombing of the WTC and the Murrah Building, the method of attack was through the use of a vehicular bomb that gained close access to the building. Additional vehicular attacks have been made on U.S. embassies and military facilities located in foreign countries. The challenge for structural engineers is to develop methods for analysis and design of structures exposed to blasts. While there are current design codes for conventional loads, these standards cannot predict the loading that occurs from a terrorist attack. A blast load occurs in a matter of milliseconds and requires its own set of equations and criteria.

Significant research has been conducted over the past five decades to determine methods to predict the intensity of blast loading on structures and also methods for accurate structural analysis from these extreme load cases. However, until recently, the focus of this research has been on the effect of nuclear weapons. With the end of the Cold War and the disarming of the nuclear arsenal, the focus of blast mitigation has switched from nuclear weapons to smaller attacks on the ground from terrorists. Now this research must be reviewed and applied to the prediction of blast loads near the ground and structural response to this high level of loading.

In this thesis a method for determining the load experienced by a structure from a

terrorist blast threat on the ground will be presented and applied to a steel blast cubicle. The manual *Structures to Resist the Effects of Accidental Explosions, Army TM 5-1300* (1990) will be used to predict the pressure loading. Additional theoretical analysis will predict the acceleration, velocity, and deflection resulting from the blast. The results from these procedures will be compared to experimental data from blast tests on the blast cubicle.

Chapter 2: Background and Literature Review

2.1 Nature of Explosions

An explosion is defined as a rapid release of energy over a short period of time resulting in a pressure wave traveling away from the source. The energy may originally be stored in forms such as chemical or nuclear materials (Baker, 1983). When detonated the explosive material is converted into a high pressure gas which results in a pressure front expanding out radially from the source. This pressure front is called a blast or shock wave and is characterized by an instantaneous increase from ambient pressure to a maximum overpressure, or in the case of a free air burst the maximum positive incident pressure. The overpressure is the overall difference between the blast pressure and ambient pressure at any given time after blast detonation while the incident pressure is the pressure resulting from a free air burst. A free air burst is an explosion that has no contact with the ground before striking an object. Both pressures may be either positive or negative.

As the shock front continues to expand and reach greater distances, the incident pressure at the front decreases, and the duration of the pressure increases as shown in Figure 2-1. Also as the shock wave expands radially outward, the velocity of the shock front decreases. The gas molecules which make up the front travel at a slower velocity and contribute to the dynamic pressure. The dynamic pressure is an actual pressure and is a measure of the kinetic energy of a certain volume of air behind the shock front.

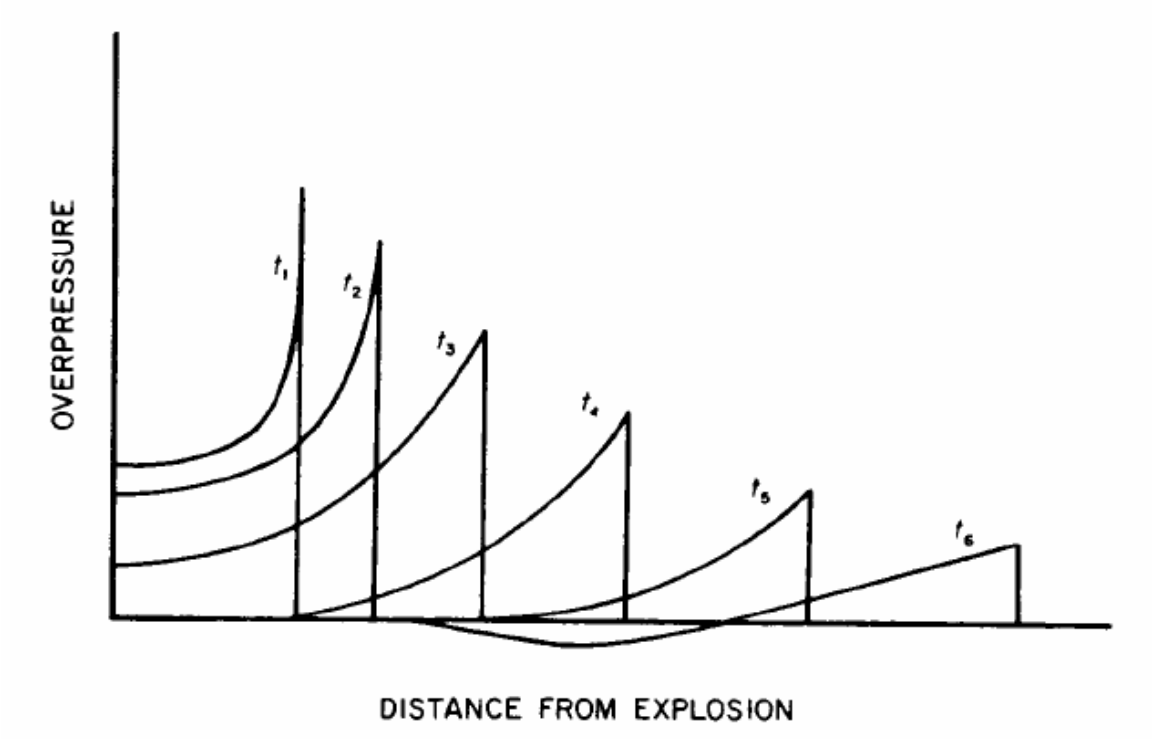

Figure 2-1 Variation of overpressure in air with distance at successive time (Glasstone, 1977)

Thus, if the air is moving the dynamic pressure is positive and if the air is not moving the dynamic pressure is zero (Glasstone, 1977).

At any particular point from the blast, the pressure profile may be represented as shown in Figure 2-2. For a short period after the detonation there is no change from the ambient pressure as it takes time for the shock front to reach the given location. At the time of arrival, t_a , the pressure suddenly jumps to that of the incident pressure and then exponentially decays to the ambient pressure condition. This part of the curve is called the positive phase duration. This is followed by the negative phase during which a suction of the air takes place and usually lasts much longer than the positive phase. At the completion of the negative phase the pressure will return to ambient pressure conditions. The maximum negative pressure is usually small compared to the incident pressure and is therefore not generally considered when designing for blast loads. The overpressure is related to the ambient pressure conditions and thus, when the negative phase is entered, is merely an indication that the pressure has dropped below ambient conditions (Glasstone, 1977; Mays and Smith, 1995; TM 5-855-1, 1986).

Another parameter associated with the pressure profile is the impulse which is designated as the area under the pressure-time curve. Separate incident values are reported for the positive and negative phase of the pressure profile. An additional consideration sometimes required for the analysis of structures is the wave length. The positive wave length is the length at a particular distance from the blast, at a particular instant of time, experiencing positive pressure. The negative wavelength is similarly defined for negative pressures (TM 5-1300, 1990).

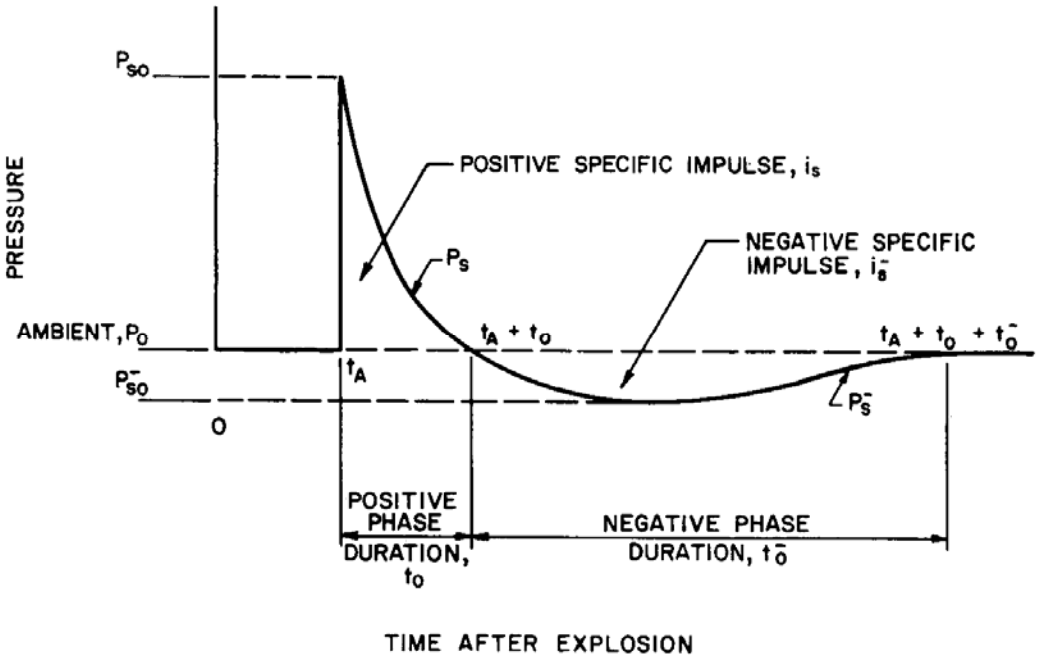

Figure 2-2 Profile for ideal blast wave (TM 5-1300, 1990)

2.1.1 Dynamic Pressure

While the overpressure is generally of most concern, there are cases where the dynamic pressure loading due to the strong winds acting with the blast wave may cause more damage. The dynamic pressure is a function of the wind velocity and the density of the air behind the shock wave. Similar to the positive overpressure, the dynamic pressure decreases with increased distance from the center of the explosion, though at a slower rate. As the overpressure changes with time so does the wind and the accompanying dynamic pressure. When the shock front arrives at a location a strong wind accompanies it blowing away from the source of the explosion. The wind velocity will decrease as the overpressure decreases but continues to blow away from the source for a period even after the overpressure has entered the negative phase. While the overpressure enters a

negative phase, the dynamic pressure always remains positive as it is not a pressure in relation to any other pressure, but is a measure of the energy of motion of the volume of air behind the shock front as seen in Figure 2-3. It is unrelated to the ambient pressure conditions present prior to the occurrence of the blast (Glasstone, 1977; TM 5-1300, 1990; TM 5-855-1, 1986).

2.1.2 Reflected Pressure

When a blast occurs the blast wave radiates out spherically from the center of the explosion. As this incident blast wave hits a hard surface, such as the ground, a reflected blast wave forms. The intensity of this reflected pressure is dependent on the strength of the incident wave and the angle at which the wave strikes the surface, called the angle of incidence. When the shock wave strikes a surface that is perpendicular to the direction of travel of the shock wave then the maximum reflected pressure will form. This total

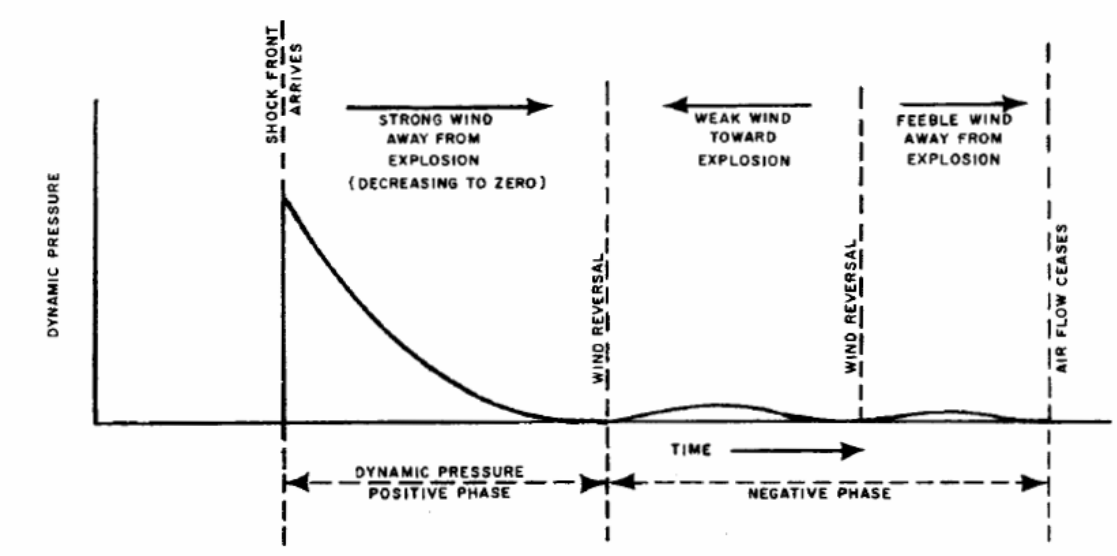

Figure 2-3 Variation of dynamic pressure with time at a given location (Glasstone, 1977)

overpressure after reflection may be as much as twice the strength of the incident pressure. The reflected pressure will vary from this maximum value, in the case of a perpendicular surface, to the minimum where the struck surface is parallel to the direction of the shock wave and objects will only experience the incident pressure.

At the ground surface one blast wave, primarily the reflected wave, will be felt by objects. However, at a certain location above the surface two different shock waves will be felt: first the incident wave and then only seconds later the reflected blast wave as shown in Figure 2-4 and Figure 2-5. Because the incident blast wave has heated the air in its passing, the reflected wave will always travel at a faster speed and will eventually overtake and merge with the incident wave forming what is commonly known as a Mach

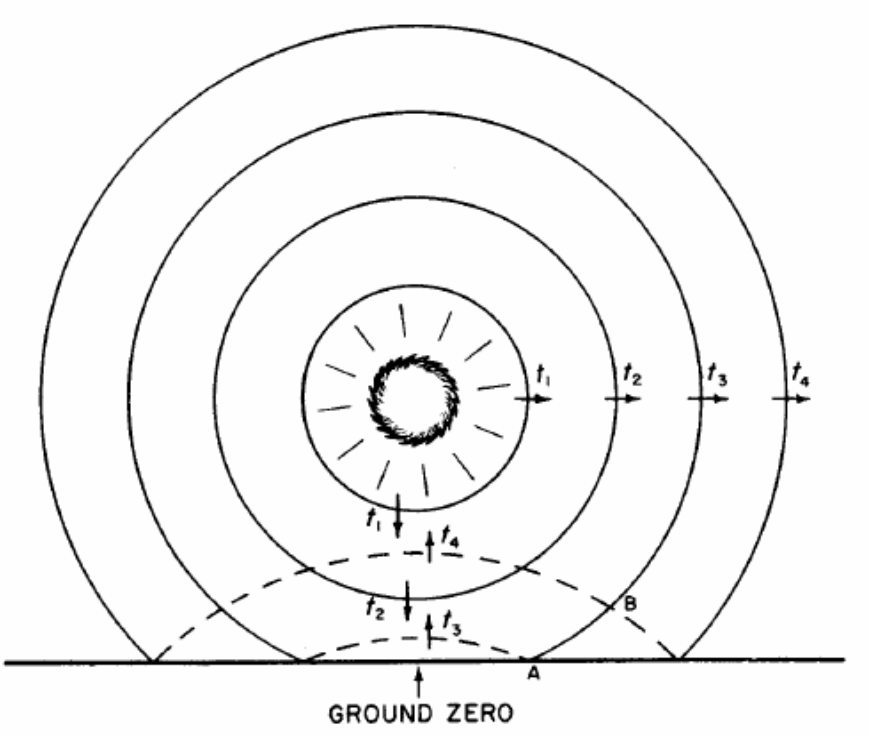

Figure 2-4 Reflection of a blast wave on ground surface (Glasstone, 1977)

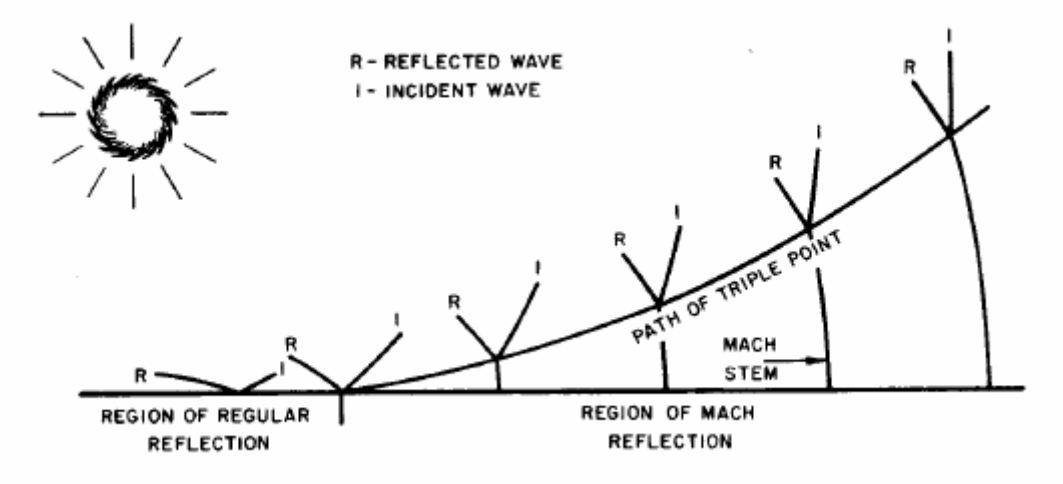

Figure 2-5 Outward motion of the blast wave near the surface in the Mach region (Glasstone, 1977)

region. The behavior of the Mach wave is the same as that described earlier for shock waves in general. The point at which these two waves merge is called the triple point. As the reflected wave takes over the incident wave the Mach stem increases in height and the triple point rises. If the two waves have not yet merged when they strike an object, in the area above the triple point, two separate blast waves will be felt (Glasstone, 1977, TM5-855-1, TM 5-1300).

2.2 Types of Burst

2.2.1 Free Air Burst

A free air burst is an explosion that has no contact with the ground before striking an object. This type of explosion is associated with nuclear weapons that are detonated at thousands of feet above the intended target. Since the detonation occurs so far from the ground there is no reflected pressure and the loading is due solely to the incident and

dynamic pressures of the blast wave (TM 5-1300, 1990).

2.2.2 Surface Burst

A surface burst occurs when an explosive is detonated on the ground or very near the ground surface. The incident wave will reflect on the ground surface to form a reflected wave. The reflected blast wave will almost instantaneously merge with the incident wave creating a Mach region at or very near the source of the explosive detonation. This type of explosion is the focus of research in regard to terrorist threats on the ground (TM 5-1300, 1990).

2.2.3 Confined Explosions

This type of explosion is seen when the blast occurs within a structure. The incident pressures of the blast wave will be very high and further amplified by reflected waves off the interior surfaces. The pressures reflected within the structure are referred to as shock pressures and are greatly reduced as venting to the outside atmosphere is increased. Thus the more openings provided in a structure the less internal damage that will occur (TM 5-1300, 1990).

2.3 General Considerations for Blast Design

2.3.1 Preventative Measures

Blast resistant design is applicable for buildings with high risks of terrorist attack such as federal office buildings, military bases, and embassies. Additionally, buildings with operations resulting in increased risk of accidental explosion, such as petrochemical

plants, should be designed for blast. When approaching blast design the first objectives should be to ensure life safety and also prevent the explosion from having a significant effect on the targeted structure. This may be accomplished by implementing systems outside the facility to prevent damage from blast effects. The first procedure is to prevent the bomb from gaining access to the facility by providing stand-off distance. While this may not be feasible in the downtown areas of cities, barriers should be implemented to negate access if possible. Possible barriers include vehicular bollards, landscaped features, decorative fences, and any other architectural feature that may be implemented into the overall design of the building and the surrounding property. Though not practical for all buildings, many government facilities that are especially prone to terrorist attack will install blast walls outside the structure to absorb the initial force of the blast before striking the building (Dusenberry, 2003; Ettouney, 1996; Marchand, 2004).

If the building is unable to have exterior barriers, restricted access should be implemented to eliminate the need for design of internal structural members for blast resistance. Personnel should be required to wear identification with badge access for interior areas of the building and visitors check-in at a main location to be escorted. Any deliveries and mail may be delivered to an offsite facility and inspected before being delivered to the intended destination. The interior allocation of space can also contribute to life safety by assigning perimeter areas with little exterior standoff distance as storage space that will have minimal occupancy (Dusenberry, 2003; Ettouney, 1996; Marchand, 2004).

While these measures may prevent many terrorist threats, they cannot avert all occurrences. It is in this arena that the structural engineer may make the greatest

contribution by preventing progressive collapse and providing protective interior and exterior walls to protect the intended victims and facilities. In order to ensure the blast resistance of structures, a thorough understanding of the behavior of blasts and the loads they apply to structures must be understood.

2.3.2 Overview of Blast Design

There are several valuable resources available which provide a broad overview of blast design. Longinow and Alfawakhiri (2003) present an overview of structural steel blast design in a question and answer format. Questions are broken into sections encompassing general explosion science, physical security, structural design, progressive collapse, structural members, and analysis methods. Ngo et al. (2007) presents an overview of the effects of explosions on structures and discusses different methods to estimate blast loads and structural response. Common equations for prediction of blast pressure and methods of analysis of buildings subjected to blast loads are presented. The author offered two case studies and used a simplified triangle shape for the blast load profile and the code LS-Dyna-3D and also performed a progressive collapse analysis.

The American Institute of Steel Construction (AISC) has published a report by Marchand and Alfawakhiri (2004) that encompasses all aspects of blast and progressive collapse steel design. This document is also presented in a question and answer format but provides more in depth information than Longinow and Alfawakhiri (2003). The general science behind blast effects are discussed along with threats and acceptable risk. Recommendations are made concerning steel structural systems and local extreme loads such as blast loads at connections. Additional information includes progressive collapse

mitigation and a history of blast and collapse events. Current and future research needs are also addressed.

2.4 Analysis Techniques

2.4.1 Prediction of blast loads

Load determination is the first step in any design or analysis process. Prediction of blast loads may be performed by hand calculations using equations and graphs provided in blast design manuals such as TM 5-1300 (1990) or TM 5-855-1 (1984). However, several computer software programs have been developed to predict the blast loads on structures. These programs incorporate the equations and graphs from a particular design manual or incorporate blast data from multiple explosive tests to predict the blast load. Commonly used blast load prediction programs include BlastX, SHOCK, SHARC, and ConWep. BlastX and ConWep are based on the Kingery and Bulmash (1984) mathematical model.

Chock and Kapania (2001) reviewed two methods for determining blast profiles for use in creating the computer program BLASTX. The two methods are from *Explosions in Air* by Baker (1973) and the method presented by Kingery and Bulmash (1984) in their article on air blasts. The methods were compared after the creation of the program and conservatively model the effects of both spherical air blast and hemispherical surface burst.

Bogosian et al. (2002) compared blast predictions from a number of programs such as BLASTX, ConWep, and SHOCK to a range of test data spanning three decades

and nearly 300 individual measurements. All of the measurements were taken at low heights, some on small cubicles and others on larger buildings. For the blast pressures, ConWep provided the best representation over the various standoff distances. SHOCK was a lower bound prediction with the majority of the test data lying above its prediction curve. On the other hand, BlastX bounded the data on the upper side and was reasonably close to the ConWep prediction. For the impulse prediction SHOCK was a clear upper bound without any data points lying above the SHOCK curve. BlastX and ConWep very closely predicted the impulses. Overall, ConWep was the best prediction method for pressure and impulse.

2.4.2 Approximate Methods

Design for blast resistance and individual structural components has traditionally been accomplished through single-degree-of-freedom (SDOF) analysis. SDOF is a linear or non-linear dynamic analysis that simplifies the structure by assuming a response mode and a response shape. This involves lumping the structure's mass at a single point and developing a spring-mass system (Marchand, 2004; Ngo, 2007; Sunshine, 2004). The equation of motion of the un-damped elastic SDOF system is given by Biggs (1964) as Equation 2-1.

$$M\ddot{y} + Ky = F_m\left(1 - \frac{t}{t_o}\right) \qquad \text{(Eq. 2-1)}$$

F_m – peak external force
K – structural stiffness
M – structural mass
t – time from beginning of loading

t_o – positive phase duration

$\ddot{y}$ - acceleration

y – displacement

The SDOF method is employed in the design manual TM5-1300 (1990) and used in the design of many military structures. Transformation factors for elements with varying support and loading conditions may be found in charts and tables in Biggs (1964) and other books concerning dynamic design.

Urgessa and Maji (2006) used an equivalent non-linear SDOF model to validate blast tests on full-scale masonry wall segments. They used step-by-step integration using the linear acceleration method to solve the non-linear equation of motion. The response in this method is evaluated at successive time increments of equal lengths of time. The measured blast wave parameters were in good agreement with the predicted blast wave parameters.

For most blast calculations the SDOF analysis is conducted with hand calculations. However the process may be expedited through the use of several SDOF software programs. Some codes available to government organizations and its contractors are SDOF, SPan32, WAC, HazL, WINLAC, and WINGARD (Sunshine, 2004).

2.4.3 Finite Element Methods

While SDOF analyses are straightforward, their simplicity can lead designers to neglect potential failure modes not assumed in the SDOF derivation. Therefore, for more complex structures, nonlinear finite element computer programs have become a common

method of dynamic analysis. Software such as ANSYS, ADINA, ABAQUS, DYNA3D, and LSDYNA allow individual structural members and connections to be considered in detail as part of a finite element model. Results from finite element calculations have been shown to compare well with test data and provide a good alternative to field tests (Crawford and Liu, 2006). While these methods are appealing, specialized training and experience is required to guarantee accurate results. The following literature provides examples of blast research conducted using finite element analysis, the list is not comprehensive.

Sparling et al. (1997) performed a study to determine the dynamic response of a steel frame industrial building to blast loads. The analysis was performed on a single frame and employed the finite element program ANSYS. Five explosions were investigated with two dynamic blast histories applied. An equivalent static loading was also used to approximate the blast load effects. Compared to the ANSYS results, the equivalent static loading accurately predicted peak bending moments in the frame but overestimated lateral deflections.

Sabuwala et al. (2005) investigated fully restrained steel connections subject to blast loads using finite element analysis. These results were then compared to requirements in TM5-1300. ABAQUS was selected and indicated as the best finite element analysis software to use based on information gathered by the author from his literature survey. Results indicate the TM5-1300 criteria are inadequate if used to judge a steel frame based solely on rotations of the structural member.

Krauthammer and Oh (1998) assessed the structural response of steel connections under blast loads and compared results to the TM 5-1300 guidelines. The finite element

code DYNA3D was used to evaluate a one-story hypothetical frame structure with welded beam-to-column connections. To determine the structural capacities of the connections, the maximum rotational deformations were investigated. The study concluded that TM 5-1300 does not consider the large local deformations of members but only plastic modulus and ultimate strength.

A study conducted by Zain (2006) analyzed a finite element model of a concrete storm shelter, designed according to FEMA 320 specifications, exposed to blast loads. The blast loads were determined using both hand calculations from the TM 5-1300 (1990) manual and the computer blast prediction software ConWep. The research studied the behavioral response of storm shelters under blast loads and the differences between the analytical results of the static and dynamic analyses. Also the ability of storm shelters to withstand blast effects at various distances was examined. The study concluded that concrete storm shelters designed according to FEMA specifications can withstand low range blast loads. However, no type of concrete storm shelter, regardless of the explosive size, can withstand a close-in explosion.

2.5 Experimental Work

Compared to numerical studies, the number of experimental studies to determine the effects of blast loads on steel structures is relatively small. Most experimental research has focused on hardened structures made of concrete or masonry. While many studies have focused on steel plates exposed to localized blast loading, the application is generally for aircraft or armored vehicles and is not related to structural design. Key issues that need further experimental research for steel structures include steel splice

configurations, connections, and base plate configurations (Marchand, 2004). Another area of research is the behavior of building frames after the removal of a beam or column due to a blast.

Lawver et al. (2003) tested AISC W14 columns to determine their structural response to blast loadings. A total of seven tests included individual columns simultaneously subjected to axial and blast loading. One test included five columns built into a frame with moment connections at the top and base plate connections at the bottom. Predictions of structural response were developed using the SDOF and FLEX finite element methods. Tests showed vulnerability of connections and plate failure under close-in blast threats. Both FLEX and SDOF predicted the peak displacement for the columns for charges far from the blast. For the near charges, the SDOF method did not accurately predict the individual flange and web responses that the FLEX analysis could capture.

Jacinto et al. (2001) compared experimental and numerical responses of plates subjected to explosive loads in order to obtain guides for modeling and analysis. The experimental results could also be used to develop design guidelines for steel bridge plated construction and offshore topsides, the surface hardware installed on offshore oil platforms. A set of four tests were conducted on two non-stiffened metallic steel plates with different boundary conditions. A time history of the acceleration of different points on both plates and the pressure waves were recorded for four separate explosive weights and standoff distances. The finite element program ABAQUS was used to model the plates.

Nonaka (2000) investigated the failure mode of a steel brace of the WTC explosion

in 1993. The blast tore holes in three reinforced-concrete slabs, leaving columns without lateral support for fifty feet in some places. In addition, a perimeter brace was torn in half and thrown into the tower. An adjacent diagonal brace was bent with the upper end of its plate shearing off its connection to the columns. The diagonal brace was considered in this investigation. The brace was seen to have undergone severe shearing along with bending near the end sections near the blast. The author progresses through mathematical formulas to prove his theory and concludes that the final rupture of the brace was caused by extensive shearing deformation at the column connection.

2.6 Design Manuals

Structural response under short-duration dynamic loads is significantly different from that under slower loading cases. Thus, the designer must consider the effects associated with such severe dynamic loading separately from the general design methods used to resist conventional loads. The following manuals provide guidance and design procedures for structures exposed to impact and explosion and use approximate SDOF systems for the calculation of dynamic structural response.

2.6.1 Structures to Resist the Effects of Accidental Explosions, TM 5-1300 (1990)

TM 5-1300 appears to be the most widely used manual by both military and civilian organizations for the design of structures exposed to explosive loads. It is approved for public release with unlimited distribution. Analysis methods and design procedures are outlined in the following chapters: 1. Introduction; 2. Blast, Fragment and

Shock Loads; 3. Dynamic Analysis; 4. Reinforced Concrete Design; 5. Structural Steel Design; and 6. Special Considerations in Explosive Facility Design. Further guidance is provided for selection of windows, doors and other entry points.

2.6.2 A Manual for the Prediction of Blast and Fragment Loadings on Structures, DOE/TIC 11268 (1992)

This manual provides guidance to engineers designing facilities exposed to air blast, ground shock, and fragment loadings from accidental explosions. It also aids in the assessment of the explosion-resistant capabilities of existing structures. The manual contains many equations and graphs for predicting blast loads that are accompanied by numerous example problems. The manual was originally developed for use at the Department of Energy (DOE) Pantex Plant that contains underground concrete facilities. While specific to the Pantex Plant, most prediction methods may be applied to other safety structures used in high explosive operations.

2.6.3 Fundamentals of Protective Design for Conventional Weapons, TM-855-1 (1986)

TM 5-855-1 is intended for engineers designing deliberately hardened military facilities exposed to conventional weapons. It includes protection criteria against penetrating weapons, contact detonations, and blast and fragmentation from standoff detonations. The user is assumed to have a basic knowledge of weapons effects and structural dynamics. Structures responding to standoff detonations in a predominantly flexural mode can be represented by a SDOF system. Transformation factors to represent

beams and slabs as SDOF systems are provided. For more complex geometries the analyst should consider using a multi-degree-of-freedom (MDOF) system or finite element representation. The ConWep blast prediction software is based on the methods presented in this manual.

2.6.4 Structural Design for Physical Security – State of the Practice Report (ASCE, 1995)

This report is for the use of civilian designers and planners wishing to include physical security considerations in designs and building retrofits. It addresses the design of structures to resist the effects of terrorist bombings and the steps taken for the design of civilian facilities. The following topics are covered: determination of the threat, structural load, behavior of structural systems, design of structural elements, design of security windows, design of security doors, design of utility openings, and retrofitting of existing structures. This report provides an excellent overview of blast design procedures but does not include specific information for predicting blast loads or designing structural details.

2.6.5 Design of Structures to Resist Nuclear Weapons Effects (ASCE Manual 42, 1985)

This manual is for use to design facilities that can resist all effects from the detonation of a nuclear weapon. Guidelines are included for weapon bursts in the air or at the ground surface, weapon burst locations that produce peak overpressure from tens of psi up to a few hundreds of psi, and weapon yields from kilotons to a few megatons.

Procedures and data provide guidance primarily for hardening of industrial facilities and personnel shelters. This manual provides conservative design ductility ratios for flexural response. While an excellent source for general blast design concepts, it does not provide specific guidelines for various issues such as structural details.

Chapter 3: Blast Loading

Through decades of research many methods for determining blast loads have been presented. Generally the values for incident pressure and positive impulse are required for determining loads on a structure. In order to calculate the incident pressure the parameters of equivalent blast weight and scaled distance must first be established. In the calculation of the dynamic and reflected pressures the velocity of the shock front and the density of the air behind the front are required. These parameters have been incorporated in TM 5-1300 (1990) for the determination of external blast loading on structures.

3.1 Blast Pressure Parameters

3.1.1 Equivalent TNT weight

Equations related to blast pressure correlate the distance to the center of a blast, or standoff distance, with a charge weight of TNT explosive. If a different explosive is used then it must first be converted to an equivalent TNT weight as shown in Equation 3-1 (TM5-1300, 1990).

$$W = \frac{H_{\exp}}{H_{TNT}} W_{\exp} \qquad \text{(Eq. 3-1)}$$

H_{exp} - heat of detonation of explosive in question

H_{TNT} - heat of detonation of TNT

W - effective charge weight

W_{exp} - weight of the explosive in question

The heat of detonation for many common explosives is given by TM 5-1300 (1990) as listed in Blast Scaling

The scaled distance is used to equate explosions with different charge weights and standoff distances. For example, if different weights of the same explosive are given, there will be an identical scaled distance where they will exhibit similar blast waves. The most common form of blast scaling was first presented by Hopkinson in 1915 and is referenced by Baker (1973) and takes the following form in Equation 3-2.

$$Z = \frac{R}{W^{1/3}} \qquad \text{(Eq. 3-2)}$$

Z – scaled distance

R – standoff distance

Another method is identified as Sachs scaling in Baker (1973) and is used for blasts where there are differing atmospheric pressures between the source of the explosions and the target. The equation is shown in Equation 3-3.

$$\bar{R} = \frac{R p_o^{1/3}}{E^{1/3}} \qquad \text{(Eq. 3-3)}$$

$\bar{R}$ - Sach's scaled distance

p_o - ambient pressure

E - energy of the explosive charge

The calculation results in a dimensionless number with the units of R, p, and E canceling out. Refer to

Table 3-2 for values of E for commonly used explosives.

Table 3-1. Equation 3-1 applies to unconfined explosions.

3.1.2 Blast Scaling

The scaled distance is used to equate explosions with different charge weights and standoff distances. For example, if different weights of the same explosive are given, there will be an identical scaled distance where they will exhibit similar blast waves. The most common form of blast scaling was first presented by Hopkinson in 1915 and is referenced by Baker (1973) and takes the following form in Equation 3-2.

$$Z = \frac{R}{W^{1/3}} \qquad \text{(Eq. 3-2)}$$

Z – scaled distance

R – standoff distance

Another method is identified as Sachs scaling in Baker (1973) and is used for blasts where there are differing atmospheric pressures between the source of the explosions and the target. The equation is shown in Equation 3-3.

$$\overline{R} = \frac{R p_o^{1/3}}{E^{1/3}} \qquad \text{(Eq. 3-3)}$$

$\overline{R}$ - Sach's scaled distance

p_o - ambient pressure

E - energy of the explosive charge

The calculation results in a dimensionless number with the units of R, p, and E canceling out. Refer to

Table 3-2 for values of E for commonly used explosives.

Table 3-1 Heat of detonation and heat of combustion (adapted from TM 5-1300, 1990)

Explosive		Heat of Detonation, H_{exp} (ft-lb/lb)	Heat of Combustion (ft-lb/lb)
Name	Symbol		
Baratol	-	1.04E+06	
Boracitol	-	5.59E+06	
	BTF	2.37E+06	
Composition B	Comp B	2.15E+06	3.91E+06
Composition C-4	Comp C-4	2.22E+06	
Cyclotol 75/25	-	2.20E+06	3.68E+06
	DATE/DATNE	1.76E+06	4.08E+06
	DIPAM	1.89E+06	
	DNPA	1.48E+06	
	EDNP	1.72E+06	
	FEFO	2.03E+06	
	HMX	2.27E+06	3.31E+06
	HNAB	2.06E+06	
	HNS	1.99E+06	
	LX-01	2.41E+06	
	LX-02-1	1.99E+06	
	LX-07	1.99E+06	
	LX-08	2.77E+06	
	LX-09-0	2.24E+06	
	LX-10-0	2.17E+06	
	LX-11	1.72E+06	
	LX-14	2.20E+06	
	NG	2.22E+06	2.26E+06
	NQ	1.49E+06	2.79E+06
Octol 70/30	-	2.20E+06	3.81E+06
	PBX-9007	2.18E+06	
	PBX-9010	2.06E+06	
	PBX-9011	2.14E+06	
	PBX-9205	2.04E+06	
	PBX-9404	2.18E+06	
	PBX-9407	2.24E+06	3.31E+06
	PBX-9501	2.22E+06	
Pentolite 50/50	-	2.14E+06	
	PETN	2.31E+06	2.70E+06
	RDX	2.27E+06	3.20E+06
	TETRYL	2.11E+06	4.08E+06
	TNETB	2.34E+06	
	TNT	1.97E+06	5.05E+06

Table 3-2 Properties of different explosives (Chock, 2001)

Explosive	Specific Gravity	Density, ρ_E ($lb_m sec^2/in^2$)	Weight-Specific Energy, E/W (in-lb_f/lb_m)	Volume-Specific Energy, E/V (in-lb_f/in^3)	Radius, r, of 1-lb sphere, inches
Pentolite (50/50)	1.66	1.551E-04	2.050E+07	1.23E+06	1.584
TNT	1.60	1.496E-04	1.813E+07	1.05E+06	1.604
RDX	1.65	1.542E-04	2.150E+07	1.28E+06	1.588
Comp. B	1.69	1.580E-04	2.080E+07	1.27E+06	1.575
HBX-1	1.69	1.580E-04	1.542E+07	9.44E+05	1.575

Sachs scaling would be used for explosives such as nuclear weapons that are detonated at elevations of thousands of feet above the target. For blast design to resist terrorist ground attacks, no significant change in atmospheric pressure would occur. Thus Hopkinson scaling will be used for most cases of structural design.

3.2 Loadings from a blast

3.2.1 Incident pressure

The incident pressure is the maximum positive overpressure experienced during the free air blast. Several studies have been conducted and the following equations derived for calculating this value. In some instances the positive phase duration of the blast was calculated along with other time parameters.

3.2.1.1 Brode

The earliest version of the incident pressure equation was introduced by Brode (1955) for spherical blast waves as shown in Equation 3-4 and 3-5.

$$P_{so} = \frac{6.7}{Z^3} + 1bar \qquad (P_{so} > 10 \text{ bar}) \qquad \text{(Eq. 3-4)}$$

$$P_{so} = \frac{0.975}{Z} + \frac{1.455}{Z^2} + \frac{5.85}{Z^3} - 0.019 bar \quad (0.1 \text{ bar} < P_{so} < 10 \text{ bar}) \quad \text{(Eq. 3-5)}$$

P_{so} – peak positive incident pressure (bars)

Z – scaled distance (m/kg$^{1/3}$)

3.2.1.2 Newmark

For an explosive detonated at the ground surface Newmark (1972) introduced the following formulas: one for calculation of incident pressure and the other for the positive phase duration of the blast as presented in Equations 3-6, 3-7, 3-8, and 3-9.

$$P_{so} = 6784 \frac{W}{R^3} + 93 \left(\frac{W}{R^3} \right)^{1/2} \quad \text{(Eq. 3-6)}$$

$$t_o = 10 W^{1/3} \text{ , but not less than } 2\ t_i \quad \text{(Eq. 3-7)}$$

$$t_i = \frac{10.23 W^{1/3}}{P_{so}^{1/2}} \qquad \text{for } P_{so} < 70 \text{ bar} \quad \text{(Eq. 3-8)}$$

$$t_i = \frac{20.77 W^{1/3}}{P_{so}^{2/3}} \qquad \text{for } P_{so} \geq 70 \text{ bar} \quad \text{(Eq. 3-9)}$$

P_{so} – peak positive incident pressure (bars)

R - standoff distance (m)

t_o – duration of positive phase of blast pressure (msec)

t_i – intercept on time axis of a triangle with maximum pressure P_{so} having a total area or impulse equal to the impulse of the blast pressure-time curve (msec)

W – effective charge weight (metric tons, 1 metric ton = 1000kg)

Notice here t_o is the time corresponding to the actual positive phase duration of the blast loading. The value t_i is a fictitious time used to calculate the positive impulse, i_s,

based on a linear simplification of the blast pressure curve, such that i_s is equal to the actual positive impulse.

3.2.1.3 Mills

A more recent proposed calculation for incident pressure and incident positive impulse is cited in Mills (1987) and shown in Equations 3-10 and 3-11.

$$P_{so} = \frac{1772}{Z^3} - \frac{114}{Z^2} + \frac{108}{Z} \qquad \text{(Eq. 3-10)}$$

$$i_s = 0.0093 \frac{W^{2/3}}{R} \qquad \text{(Eq. 3-11)}$$

i_s – positive phase impulse equal to the area under the pressure time curve for P_{so} (Nsec/m^2)

P_{so} – peak positive incident pressure (kN/m^2)

R – standoff distance (m)

W - effective charge weight (kg)

Z – scaled distance (m/kg$^{1/3}$)

3.2.2 Maximum Negative Pressure

The maximum negative pressure is relatively small in comparison to the incident pressure and is generally not of concern when determining the loads from a blast. There is however one author (Brode, 1955) that presented an equation for this value as follows:

$$P_{so}^{-} = -\frac{0.35}{Z} \qquad \text{for } Z > 1.6 \qquad \text{(Eq. 3-12)}$$

P_{so}^{-} - peak negative incident pressure (bars)

Z – scaled distance (m/kg$^{1/3}$)

3.2.3 Dynamic Pressure and Parameters

In most terrorist attacks the explosive will detonate only a few feet above the ground, thus instantaneously forming a Mach region which will be felt by nearby structures. Only in the case of a surface burst or in the Mach region below the triple point for an air burst may the equations for dynamic pressure be used (Glasstone, 1977). The various parameters at the front of the shock wave are correlated by the Rankine-Hugoniot equations.

The shock wave velocity, U, is expressed in Equation 3-13 (Glasstone, 1973; Newmark, 1972). The peak wind velocity in air, u, is shown in Equation 3-14 (Glasstone, 1973).

$$U = c_o \left(1 + \frac{6P_{so}}{7p_o} \right)^{1/2} \qquad \text{(Eq. 3-13)}$$

$$u = \frac{5P_{so}}{7p_o} \left(\frac{c_o}{\left(1 + 6P_{so}/7p_o\right)^{1/2}} \right) \qquad \text{(Eq. 3-14)}$$

c_o – ambient speed of sound (m/msec)

p_o – ambient pressure (bars)

P_{so} – peak positive incident pressure (bars)

U – shock front velocity (m/msec)

u – peak wind velocity behind the shock front (m/msec)

The dynamic pressure and dynamic pressure duration from Newmark (1972) are given in Equations 3-15, 3-16, and 3-17.

$$q = P_{so} \left(\frac{2.5P_{so}}{7p_o + P_{so}} \right) \qquad \text{(Eq. 3-15)}$$

$$t_i' = 9.04 \frac{W^{1/3}}{P_s^{1/3}} \qquad \text{for } P_{so} < 2\text{bar} \qquad \text{(Eq. 3-16)}$$

$$t_i' = 14.35 \frac{W^{1/3}}{P_s} \qquad \text{for } P_{so} \geq 2\text{bar} \qquad \text{(Eq. 3-17)}$$

p_o – ambient pressure (bars)

P_{so} – peak positive incident pressure (bars)

q – dynamic pressure (bars)

t_i' – drag impulse duration (msec)

W – effective charge weight (metric tons, 1 metric ton = 1000kg)

Equation 3-18 for dynamic pressure was given by Glasstone (1973).

$$q = \frac{5}{2}\left(\frac{P_{so}^{\ 2}}{7p_o + P_{so}} \right) \qquad \text{(Eq. 3-18)}$$

p_o – ambient pressure (bars)

P_{so} – peak positive incident pressure (bars)

q – dynamic pressure (bars)

3.2.4 Reflected Pressure

For a blast occurring in air, and related to the incident pressure, the reflected pressure from Glasstone (1973) is shown in Equation 3-19.

$$P_r = 2P_{so} \frac{7p_o + 4P_{so}}{7p_o + P_{so}} \qquad \text{(Eq. 3-19)}$$

p_o – ambient pressure (bars)

P_{so} – peak positive incident pressure (bars)

P_r – peak positive normal reflected pressure (bars)

Newmark (1972) offers an alternative form for the reflected pressure dependent on the

value of incident pressure in Equation 3-20 and 3-21.

$$P_r = P_{so}\left(2 + \frac{6P_{so}}{P_{so} + 7p_o}\right) \qquad \text{for } P_{so} < 10 \text{ bar} \qquad \text{(Eq. 3-20)}$$

$$P_r = P_{so}\left(4\log P_{so} + 1.5\right) \qquad \text{for } P_{so} > 10 \text{ bar,} \qquad \text{(Eq. 3-21)}$$

P_r/P_{so} should not be taken greater than 14

p_o – ambient pressure (bars)

P_{so} – peak positive incident pressure (bars)

P_r – peak positive normal reflected pressure (bars)

The equation for reflected pressure and reflected impulse for Mills (1987) is shown in Equation 3-22 and 3-23.

$$P_r = 2P_{so}\frac{\left(710 + 4P_{so}\right)}{\left(710 + P_{so}\right)} \qquad \text{(Eq. 3-22)}$$

$$i_r = i_s\left(\frac{2P_{so} + P_r}{2P_{so}}\right) \qquad \text{(Eq. 3-23)}$$

i_s - positive phase impulse equal to the area under the pressure time curve for P_{so} (Nsec/m^2)

i_r – unit positive normal reflected impulse (Nsec/m^2)

p_o – ambient pressure (kN/m^2)

P_{so} – peak positive incident pressure (kN/m^2)

P_r – peak positive normal reflected pressure (kN/m^2)

3.2.5 Blast Pressure Profile

The blast pressure profile for an ideal blast wave in free air for the positive phase of the blast may be described by the modified Friedlander equation as presented in Baker (1973) as Equation 3-25. Design curves in Baker et al. (1983) provide values for the

parameters in Equation 3-25.

$$p(t) = p_o + P_{so}\left(1 - \frac{t}{t_o}\right)e^{-b\frac{t}{t^o}} \qquad \text{(Eq. 3-25)}$$

b – decay coefficient

p(t) – blast pressure with time

t – time measured from time of arrival of blast wave

3.3 TM 5-1300: External Blast Loading on Structures

The army manual TM 5-1300 is widely used by military and civilian organizations and provides design and analysis procedures for all aspects of blast resistant design. TM 5-1300 is based on the Kingery and Bulmash (1984) mathematical model. This manual was employed for the determination of external blast loads. The blast loading on a structure is dependent on the magnitude of the explosion, the location of the explosion in relation to the structure, the geometrical configuration of the structure, and the orientation of the structure with respect to the explosion.

3.3.1 Forces acting on structure

The forces that act on a structure from a shock wave are dependent on the peak pressure and the impulse of the incident and dynamic pressures. For design purposes the actual decay of the incidental pressure is approximated by an equivalent triangular pressure pulse. The actual positive phase duration is replaced by a fictitious duration as a function of the total positive impulse and peak pressure as in Equation 3-26.

$$t_{of} = \frac{2i}{p} \qquad \text{(Eq. 3-26)}$$

t_{of} – fictitious positive phase pressure duration

i – unit positive impulse

p – pressure

Both the incident and the reflected pressures have been simplified as an equivalent triangular pulse in the positive region. The negative pressure-time phase is similary approximated as shown in Equation 3-27. The values i^- and p^- are the total impulse and peak pressure of the negative phase of either the incident or reflected blast waves.

$$t_{of}^{-} = \frac{2i^-}{p^-} \qquad \text{(Eq. 3-27)}$$

t_{of}^- - fictitious negative phase pressure duration

i^- - unit negative impulse

p^- - negative pressure

The fictitious duration of the positive phase will be smaller than the actual positive phase duration resulting in a time gap between the fictitious duration and the beginning of the negative phase. This is illustrated for a free air burst explosion with no reflection in Figure 3-1.

3.3.2 Above ground rectangular structure without openings

The following procedure is for the analysis of an above-ground rectangular structure without openings. The interaction of the blast wave with a structure may be very complicated and so several factors are assumed. The structure should be rectangular in

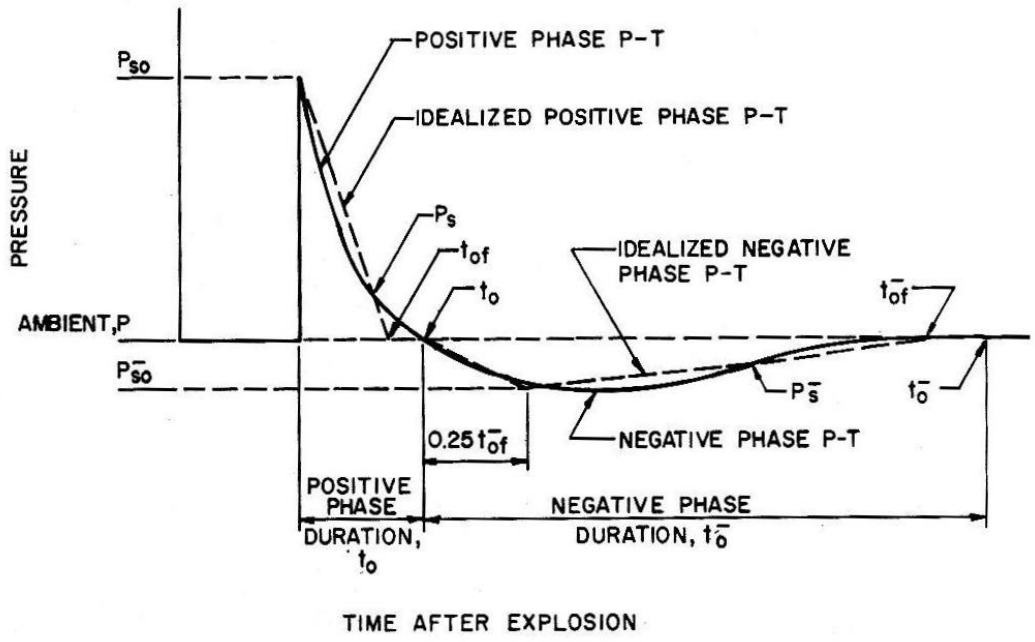

Figure 3-1 Idealized pressure-time variation for free air burst (TM 5-1300, 1990)

shape, the incident pressure is less than 200psi, and the structure is in the Mach stem region which extends above the height of the building.

3.3.2.1 Front Wall Loads

When the shock wave strikes the front wall the pressure immediately rises from zero to that of the reflected pressure, P_r, as shown in Figure 3-2. The clearing time for the reflected pressure to dissipate is indicated by the time t_c as shown in Equation 3-28. The variable C_r is found in Figure 3-3.

$$t_c = \frac{4S}{(1+R_1)C_r} \qquad \text{(Eq. 3-28)}$$

C_r – sound velocity in reflected region

H – height of structure

R_1 – ratio of S/G where G is equal to H or $W_s/2$, whichever is largest

S – height of front wall or one-half its width, whichever is smallest

t_c – clearing time for reflected pressure

W_s – width of structure

After time t_c the pressure on the wall is equal to the incident pressure and the drag pressure, P_s+C_dq. The value C_d is called the drag coefficient and is dependent on the size of the dynamic pressure, q. For the pressure region in consideration $C_d = 1$ for the front face. The value $P_{so}+C_dq_o$ will be plotted on the graph where q_o, the peak dynamic pressure, is found in Figure 3-4.

At higher pressure ranges this procedure may return a fictitious pressure-time curve because of the very short pressure pulse durations. Therefore, the pressure-time curve must be checked for accuracy. The comparison is made by plotting a second curve

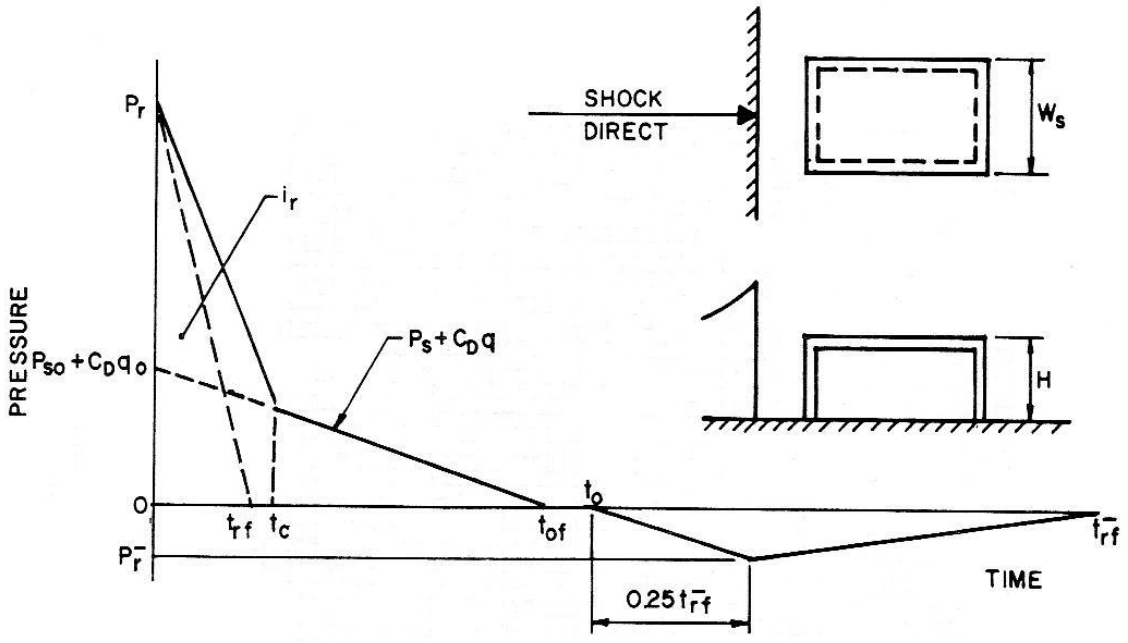

Figure 3-2 Front face loading of a rectangular structure (TM 5-1300, 1990)

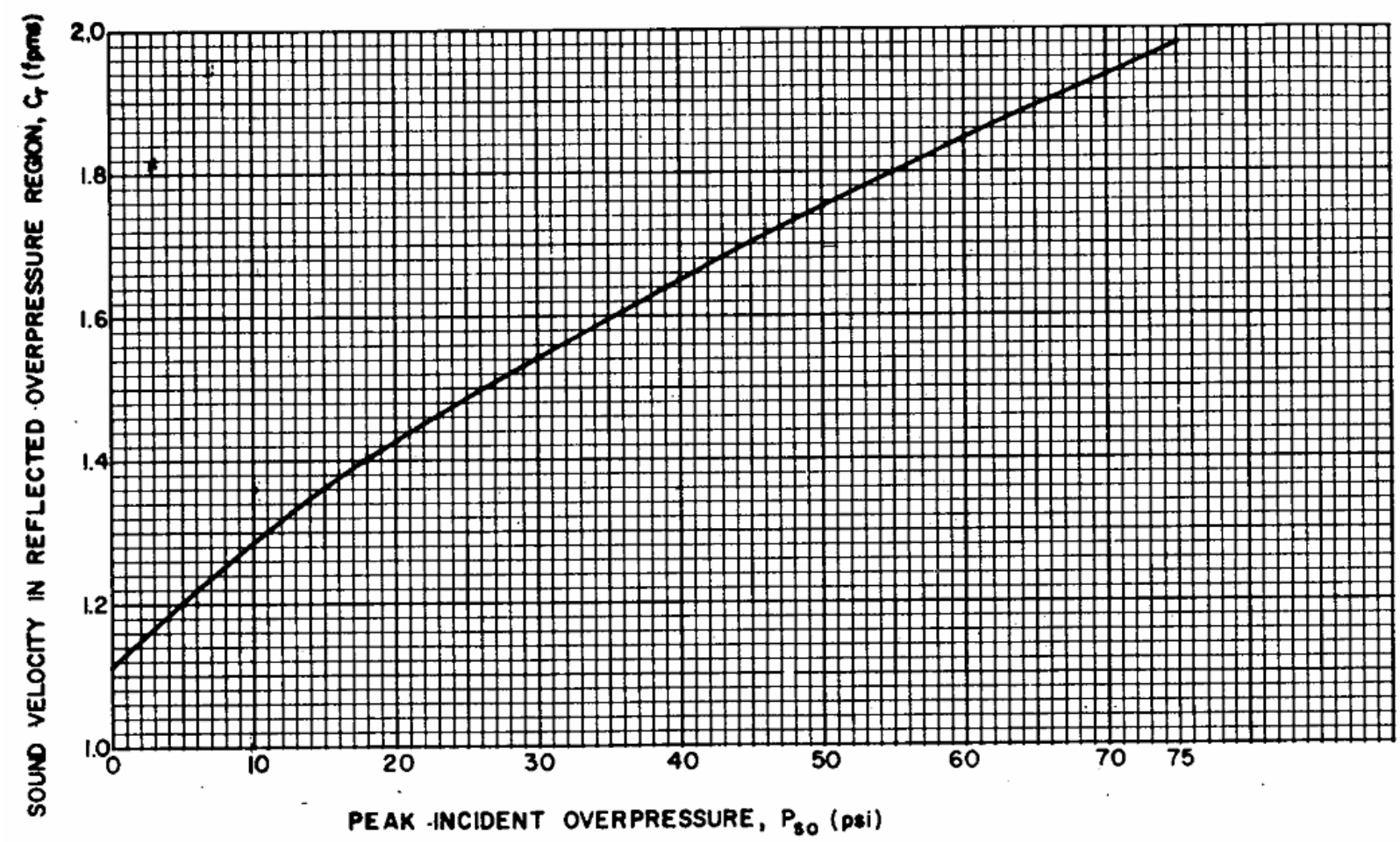

Figure 3-3 Velocity of sound in reflected overpressure region versus peak incident overpressure (TM 5-1300, 1990)

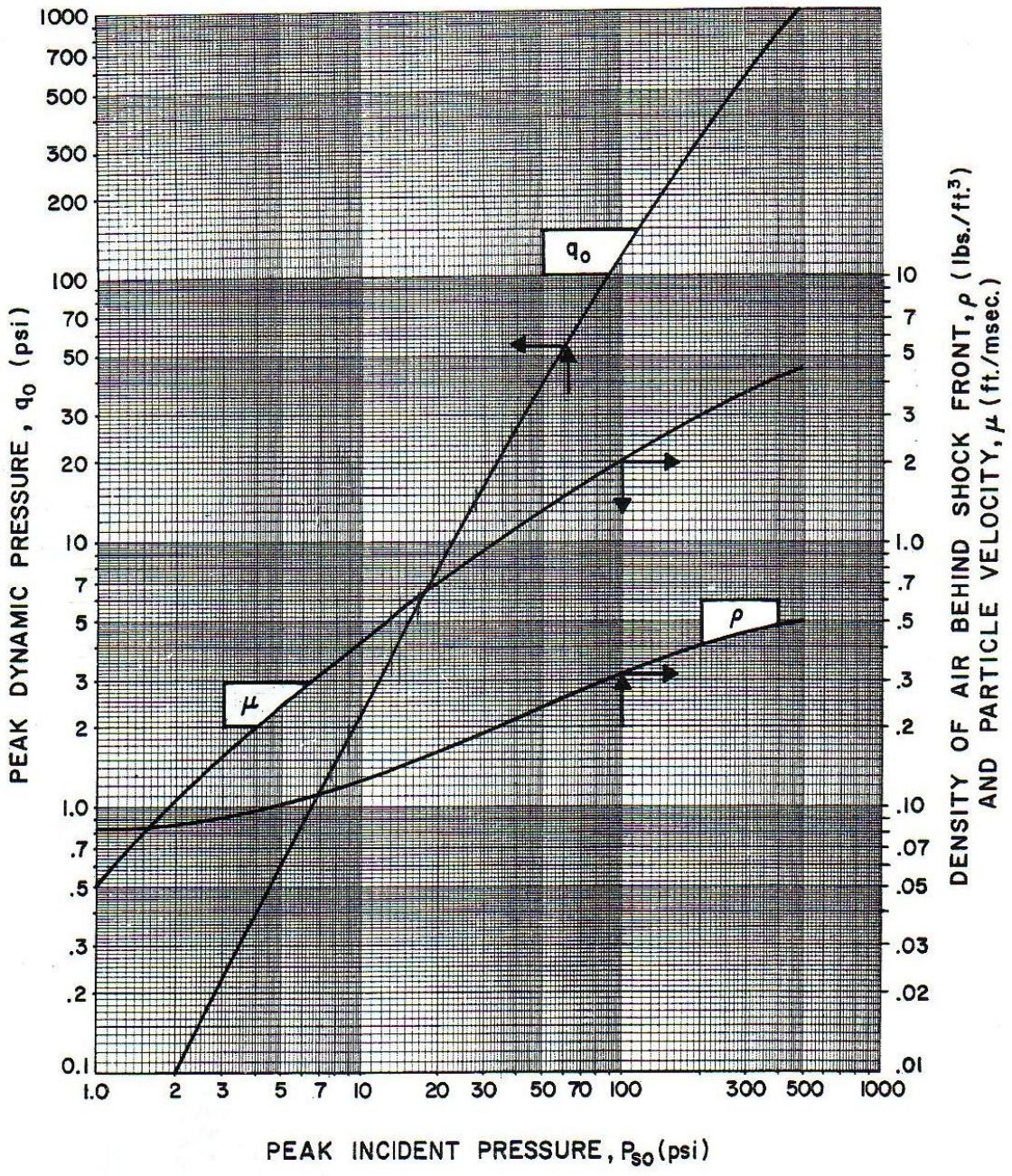

Figure 3-4 Peak dynamic pressure, density of air behind the shock front, and particle velocity versus peak incident pressure (TM 5-1300, 1990)

using the total reflected pressure impulse i_r, as shown in Figure 3-2. The fictitious pressure duration t_{rf} for the reflected wave is the time intercept for the reflected pressure impulse, Equation 3-29 shows the formula for calculating t_{rf}.

$$t_{rf} = \frac{2i_r}{P_r} \qquad \text{(Eq. 3-29)}$$

t_{rf} – fictitious reflected positive pressure duration

Whichever curve gives the smallest value for the impulse should be used in calculating the wall loading. Positive phase parameters are found in Figure 3-5.

For determining the overall motion of the structure, the negative pressures should be included. The peak negative reflected pressure and negative reflected impulse may be obtained from Figure 3-6. The rise and decay times are calculated as described for Equation 3-27 except substituting in i_r^- and P_r^-, the unit negative normal reflected impulse and peak negative normal reflected pressure, respectively. The rise time of the negative phase is equal to $0.25t_{rf}^-$, with t_{rf}^- being the fictitious reflected negative pressure duration.

3.3.2.2 Roof and Side Wall Loads

As the shock front passes a structure, a pressure is present on the roof and side walls equal to the incident pressure at a given time minus the drag pressure. The loading is dependent on the magnitude of the incident pressure, location of the shock front, and the wavelength of the positive and negative impulses. The peak value of the pressure is the sum of the equivalent uniform pressure and drag pressure as shown in Equation 3-30. P_{so} is the incident pressure acting at a particular point and q_o is the dynamic pressure corresponding to $C_E P_{so}$.

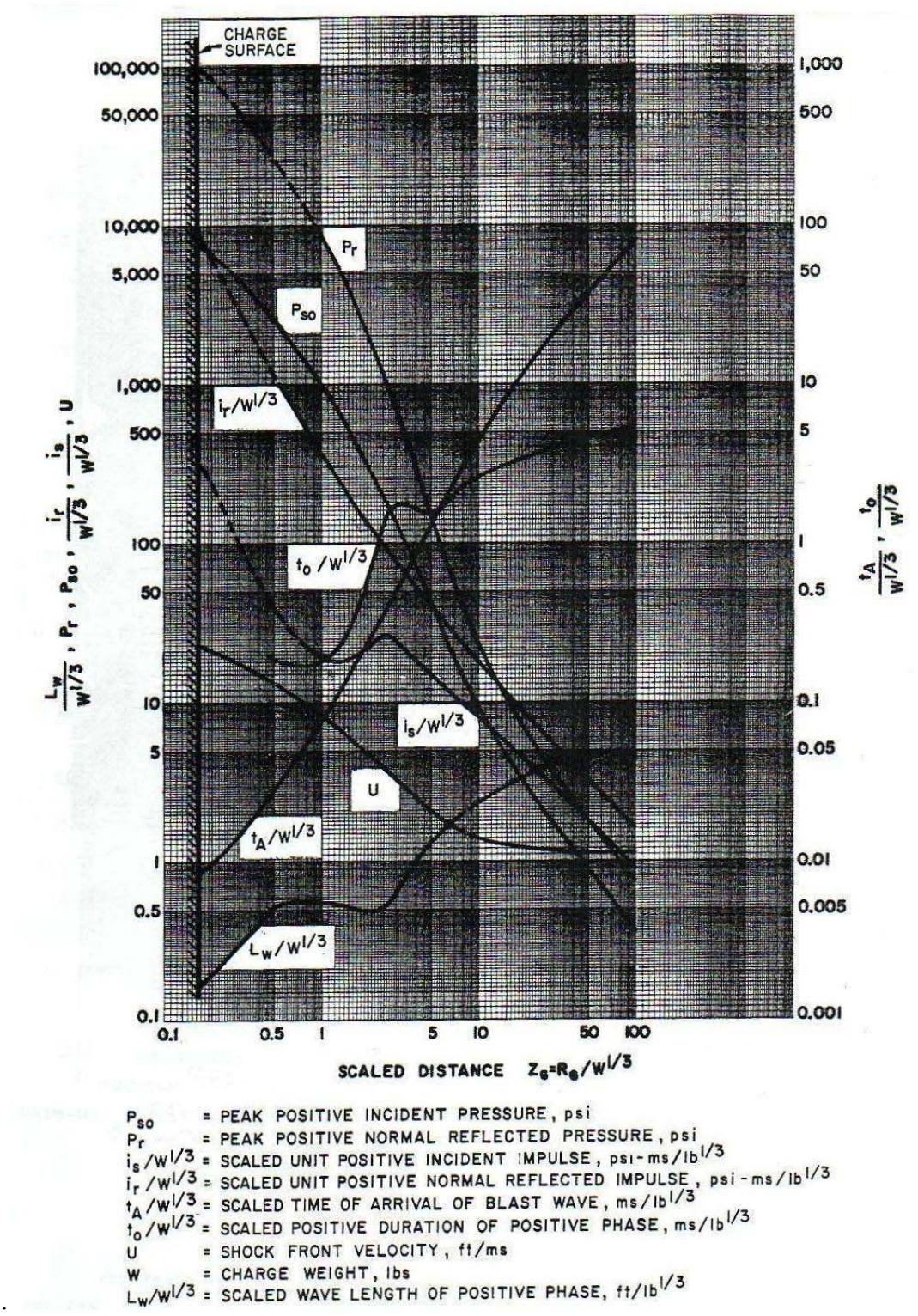

Figure 3-5 Positive phase shock wave parameters for a hemispherical TNT explosion on the surface (TM 5-1300, 1990)

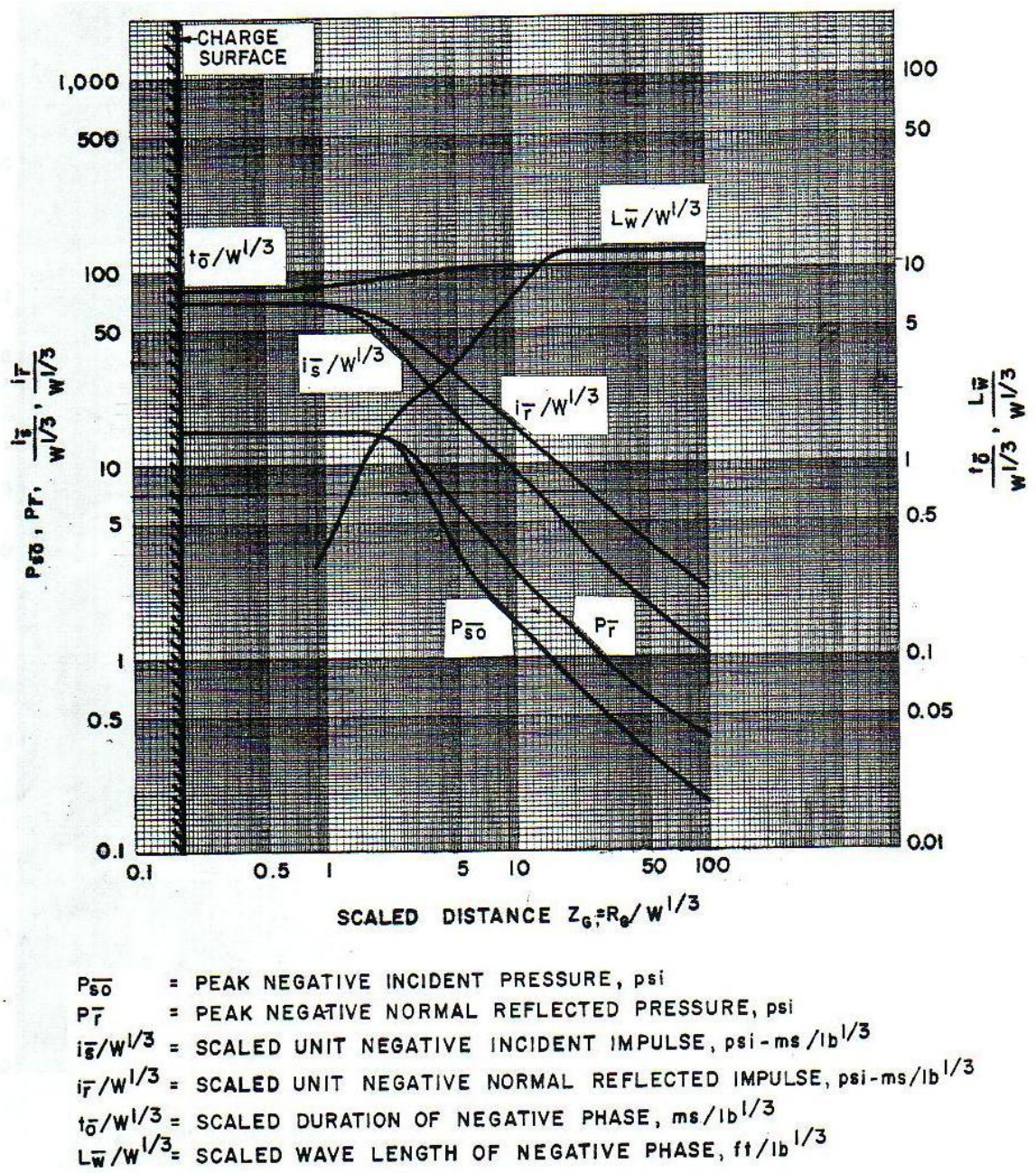

Figure 3-6 Negative phase shock wave parameters for a hemispherical TNT explosion on the surface (TM 5-1300, 1990)

$$P_r = C_E P_{so} + C_D q_o \quad \text{(Eq. 3-30)}$$

C_D – drag coefficient

C_E – equivalent load factor

The drag coefficient C_D for the roof and side walls is dependent on the peak dynamic pressure. The values in

Table 3-3 are the recommended values. Figure 3-7 presents a pressure time curve for the roof and side wall loading.

The equivalent load factor C_E, rise time t_d, and duration of the equivalent uniform pressure t_{of} are found in Figure 3-8, Figure 3-9, and Figure 3-10 as functions of L_w/L, the ratio of the wave length of the positive pressure phase over the distance between the reflecting surface and free edge in the horizontal direction. A similar procedure is conducted for the negative load. The equivalent load factor C_E for the negative pressure is in Figure 3-8. The value of the negative pressure P_r^- is equal to $C_E P_{so}$ where C_E is a negative value. The equivalent negative phase duration is obtained from Figure 3-10 and is not a function of the peak positive incident pressure. The rise time of the negative phase is equal to $0.25t_{of}^-$, where t_{of}^- is the fictitious negative phase pressure duration.

Table 3-3 Drag coefficients corresponding to peak dynamic pressure (TM 5-1300, 1990)

Peak Dynamic Pressure, q_o (psi)	Drag Coefficient, C_D
0 – 25	-0.40
25 – 50	-0.30
50 – 130	-0.20

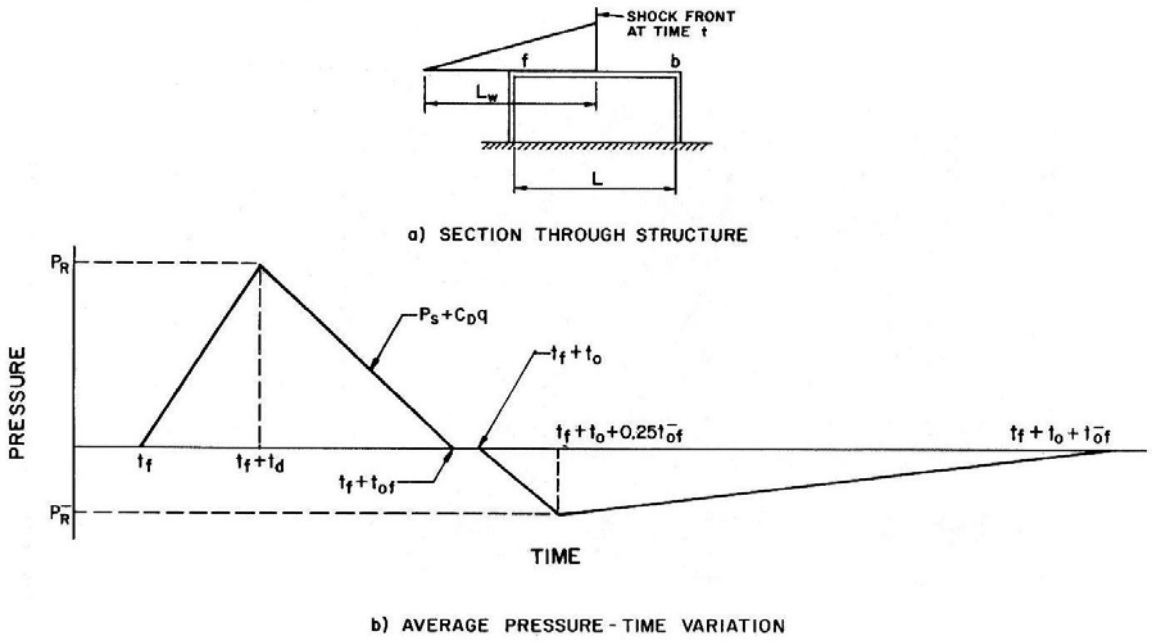

Figure 3-7 Roof and side wall loading (TM 5-1300, 1990)

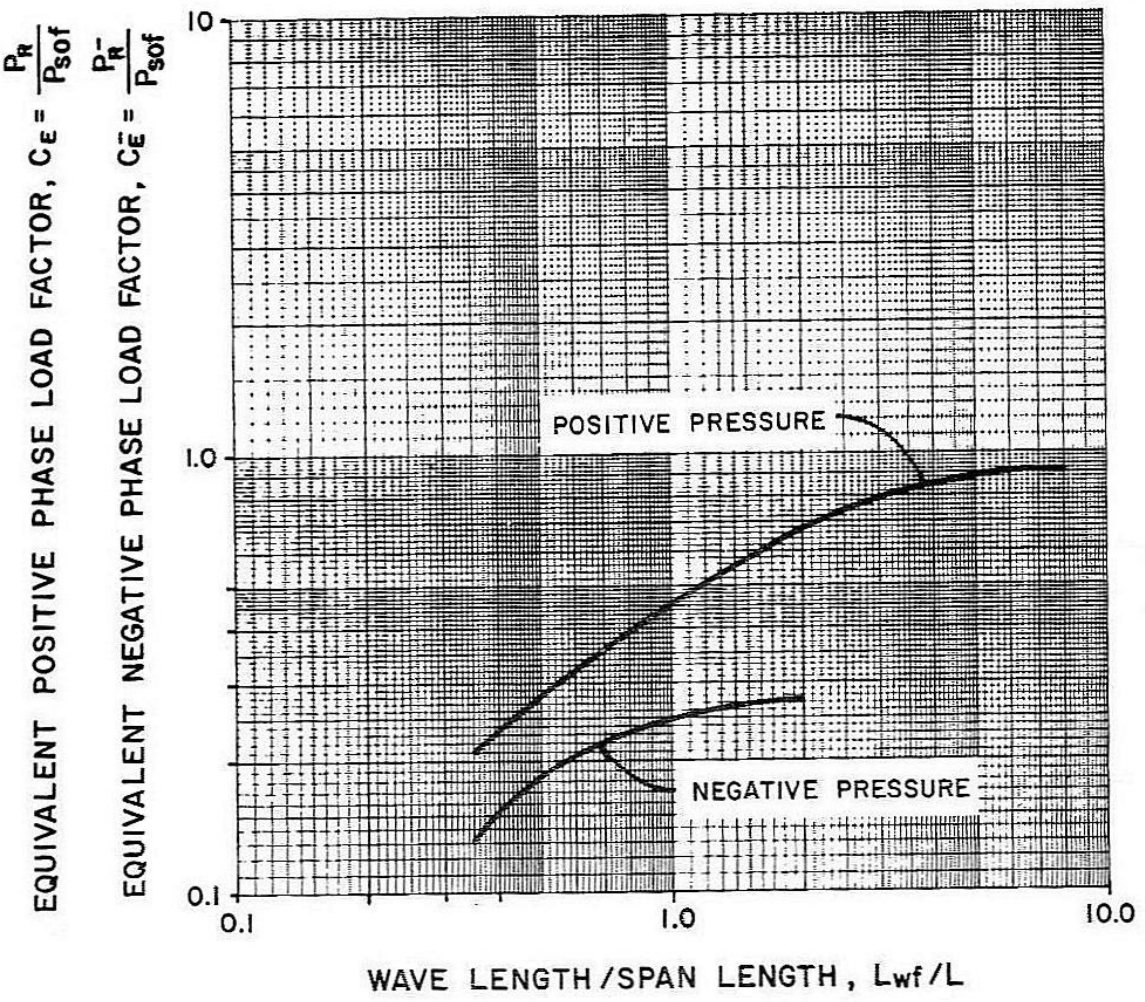

Figure 3-8 Peak equivalent uniform roof and side wall pressures (TM 5-1300, 1990)

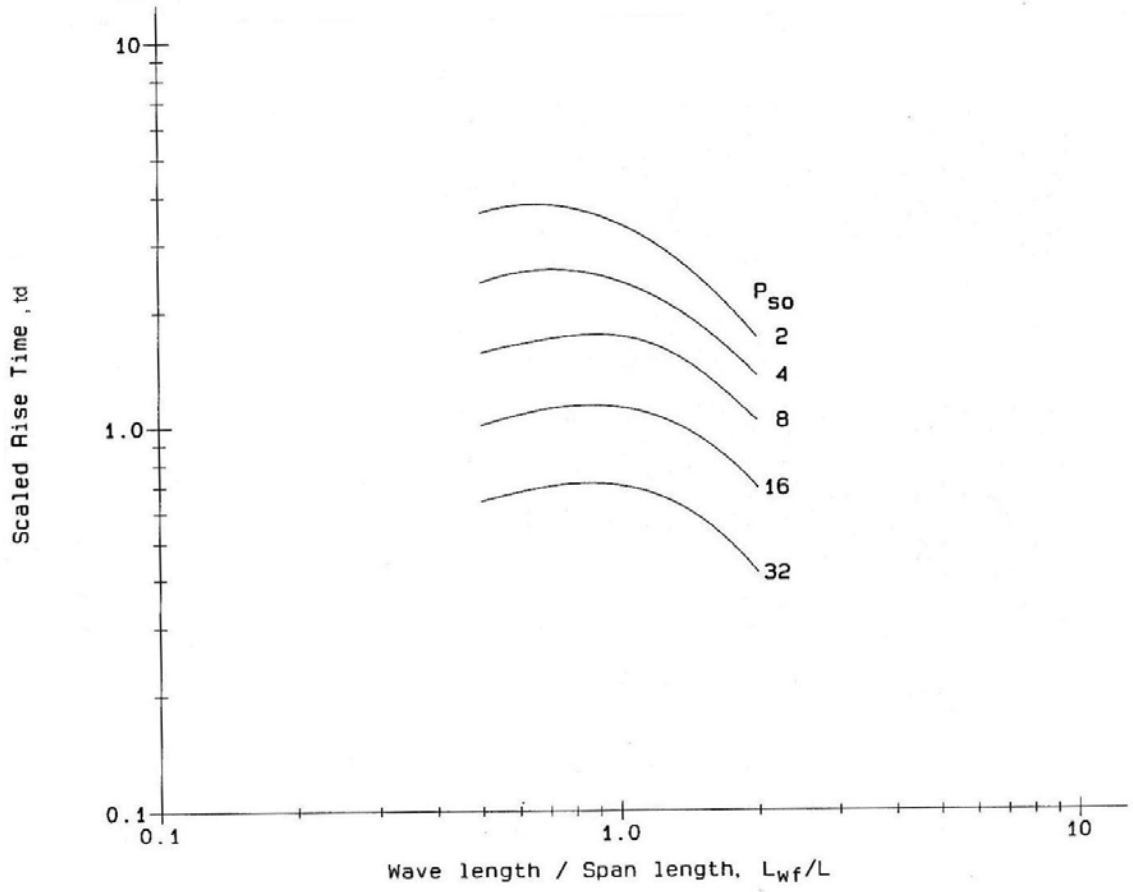

Figure 3-9 Scaled rise time of equivalent uniform positive roof and side wall pressures (TM 5-1300, 1990)

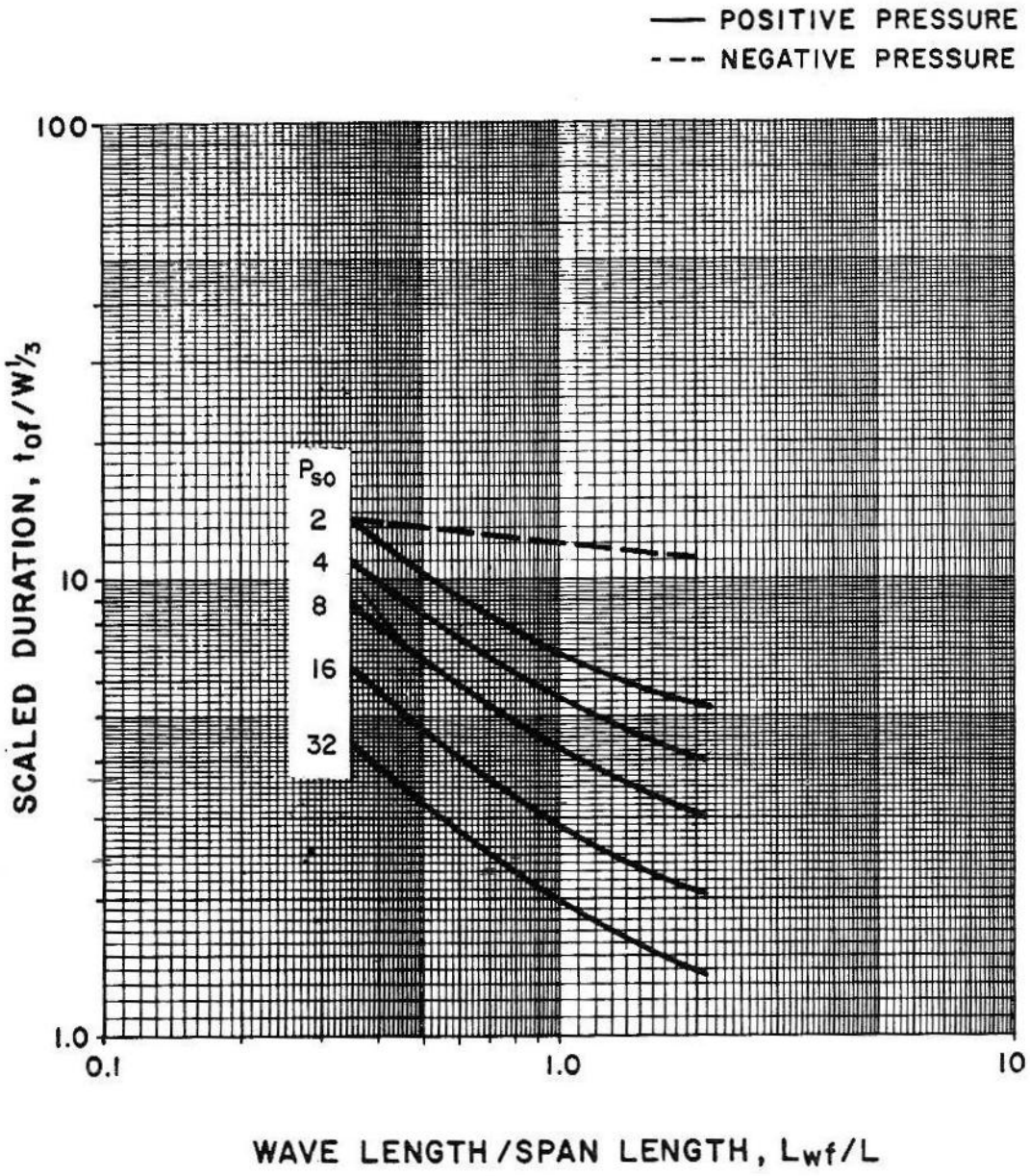

Figure 3-10 Scaled duration of equivalent roof and side wall pressures (TM 5-1300, 1990)

3.3.2.3 Rear Wall Loads

The calculation of the blast load on the rear wall is the same as for the side wall and roof loads. However, the peak pressure on the pressure time curve will correspond to the pressure occurring at the back edge of the roof slab. The equivalent uniform load factors C_E and C_E^-, height of rear wall, rise times and durations for both the positive and negative phases are based on the wave length of the peak pressure at the back of the roof slab. The blast loads applied to the back wall are a function of the drag pressures in addition to the incident pressure. The pressure corresponding to $C_E P_{so}$ is used to calculate the dynamic pressure of the drag force. The drag coefficients are the same as for the side and roof loads in

Table 3-3.

Figure **3-11** presents a pressure-time curve for the rear wall loading.

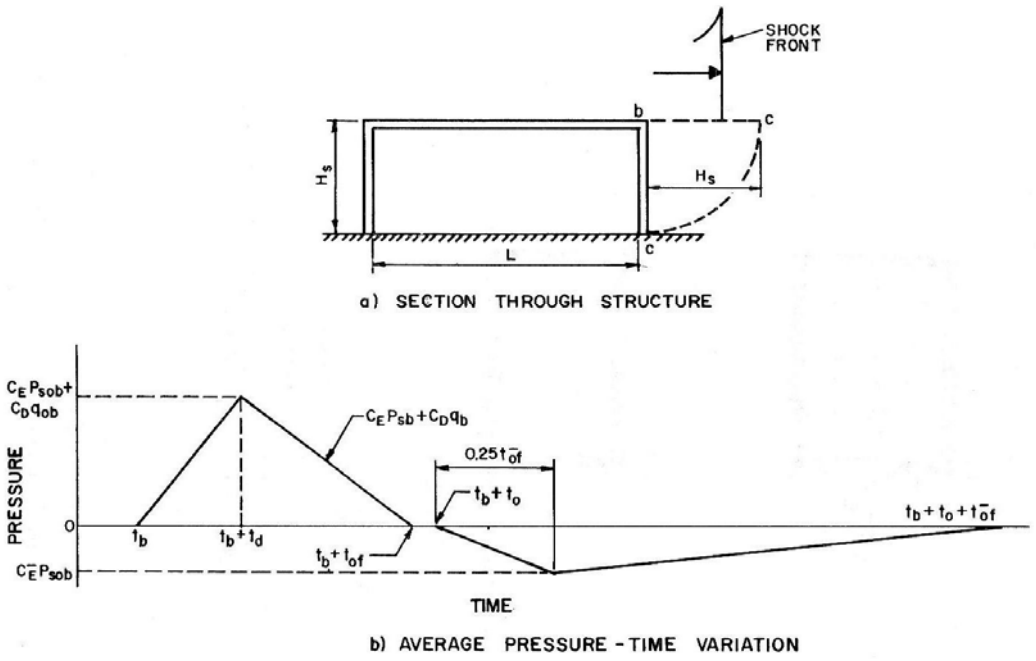

Figure 3-11 Rear wall loading (TM 5-1300, 1990)

3.3.2.4 Surface Blast Load Procedure

The following procedure should be followed to determine the blast loading from a surface burst on above-ground rectangular structures without openings:

1. Determine the charge weight W, ground distance to blast R, and structure dimensions. Calculate the scaled distance Z.
2. If designing a new structure, apply a safety factor of 1.2 to the charge weight. If determining the actual blast load experienced by a structure, use a safety factor of 1.0.
3. Select several points on the structure (front wall, halfway point of roof and side wall, rear wall) and determine the free-field blast wave parameters for each point from Figure 3-5.

4. For the front wall:

   Calculate peak positive reflected pressure P_r and positive reflected impulse $i_r/W^{1/3}$ from Figure 3-5. Multiply scaled value by $W^{1/3}$ to obtain absolute value.

5. Determine positive phase of front wall loading:

   a. Determine the sound velocity C_r from Figure 3-3 for the peak incident pressure P_{so} corresponding to the front wall.

   b. Calculate clearing time t_c in msec (equation 3-28)

   c. $$t_c = \frac{4S}{(1+R_1)C_r}$$

   d. Calculate fictitious positive phase duration t_{of}:

   $$t_{of} = \frac{2i_s}{P_{so}}$$

   e. Determine peak dynamic pressure q_o from Figure 3-4 for P_{so}.

   f. Calculate $P_{so} + C_d q_o$. For the front wall C_d is unity as mentioned in Section 3.3.2.1.

   g. Calculate the fictitious duration of the reflected pressure

   $$t_{rf} = \frac{2i_r}{P_r}$$

   h. Construct the positive pressure-time curve of the front wall similar to Figure 3-2. The actual loading is the smaller of the impulse due to the reflected pressure or cleared reflected pressure plus the incident pressure.

6. Determine negative phase of the front wall loading

a. Determine the values P_r^- and $i_r^-/W^{1/3}$ from Figure 3-6. Multiply scaled value of the negative impulse by $W^{1/3}$ to find absolute value.

b. Calculate the fictitious duration of the negative reflected pressure:

$$t_{rf}^- = \frac{2i_r^-}{P_r^-}$$

c. Calculate the rise time of the negative pressure by multiplying t_{rf}^- by 0.25

d. Construct the negative phase pressure-time curve similar to Figure 3-2.

7. Determine the positive phase of the side wall loading:

a. Calculate the wave length to span length ratio L_w/L at front of the span.

b. Read values of C_E, $t_d/W^{1/3}$ and $t_{of}/W^{1/3}$ from Figure 3-8, Figure 3-9, and Figure 3-10.

c. Determine dynamic pressure q_o from Figure 3-4 for $C_E P_{so}$.

Calculate $P_r = C_E P_{so} + C_D q_o$ (Eq. 3-30). Obtain C_D from

d. Table 3-3.

e. Construct positive phase pressure-time curve similar to **Error! Reference source not found.**.

8. Determine negative phase of side wall loading

a. Determine C_E^- and $t_{of}^-/W^{1/3}$ for the value of L_{wf}/L from step 7a and Figure 3-8 and Figure 3-10.

b. Calculate t_{of}^- and $Pr^- = C_E P_{sof}$ where C_E is a negative value.

c. Calculate rise time of the negative phase of $0.25t_{of}^-$.

d. Construct the negative pressure-time curve similar to Figure 3-10.

9. Determine the roof loading. Follow the procedure for the side wall loading.
10. Determine the rear wall loading. Follow procedure outlined for the side wall loading.

3.4 Impulsive Blast Loads

The duration of the blast wave, relative to the natural period of the structure, falls into three separate categories: long duration or quasi-static loading, intermediate or dynamic loading, and short duration or impulsive loading. Long duration loads are usually associated with nuclear blast at medium to long range. In this case the maximum displacement is dependent on the peak blast load and structure stiffness and is not a product of the positive phase duration or the structural mass. For intermediate loads, the parameters such as shape and blast wave duration affect the structural response. Short duration loads are generally over before the structure has responded. In this case the impulse, or area under the positive region of the pressure-time curve, influences the response (Smith and Hetherington, 1994). TM 5-1300 (1990) presents charts that show if the blast wave is less than 25 percent of the fundamental period then an impulsive load may be assumed with negligible error in results.

Chapter 4: Analysis and Results

This chapter is a revised version of a paper titled "Full Scale Surface Blast Test for Steel Blast Cubicle" written by Sarah Janney, Qiuhong Zhao, James Dyer, Richard Bennett, and Edwin Burdette. The paper will be submitted to the "Journal of Structural Engineering."

My primary contributions to the paper included (1) generation of pressure-time curves, (2) filtering of accelerometer data, (3) interpretation of results, and (4) most of the writing.

4.1 Introduction

Surface blast tests were carried out at The Hurricane Test Laboratory (HTL) in Lubbock, Texas as part of a project to determine the blast resistant capabilities of steel blast cubicles. Analytical and numerical modeling methods verified the tests.

The blast cubicles are designed to provide protection for personnel in areas of potential terrorist activity. In the case of an explosion, the blast cubicle must withstand the blast and provide life-safety for those inside. Terrorist bomb attacks commonly target military facilities where most existing buildings are not designed to resist blast loading. In cases where blast shelters have been erected, they are permanent buildings made of concrete or masonry and are often located underground. While effective, these facilities are not practical for use in mobile military facilities where buildings must be transportable and easily constructed.

The blast cubicle is a modified version of modular buildings designed for in-residence and community F-5 tornado shelters built to withstand wind speeds up to 250mph. The blast cubicle is a light gauge steel structure and is easily assembled by two

people under field conditions with standard tools, disassembled, and transported to new areas of operation. The portability of the structure allows for use in mobile military field operations. Experimental testing determined the blast load experienced at different standoff distances and the blast resistance capability of the blast cubicle.

4.2 Specimens and Test Setup

The blast cubicle is made of galvanized cold rolled steel and has outside dimensions of 94 in x 94 in x 94 in as shown in Figure 4-1. The cubicle has four walls, a roof, a floor, and a door opening in the rear wall. The walls, roof, and floor consist of 18 gage (0.0516 in) channels connected together using No. 12 hex headed screws at 16" on center. The wall channels are respectively sheathed on the outside and inside with 12 gage (0.1084 in) and 16 gage (0.0635 in) panels using Sikaflex adhesive. The roof and floor have no outside or inside panels but the floor is overlain with plywood. Section details without panels attached are shown in Figure 4-2. The cavities of the wall were filled with sand through holes in the top tube frame of the wall. Neither the floor nor roof was filled with sand. While QUIKRETE Playsand Product Number 1113 was used for the blast test, existing sand or soil may be used in field operations. The blast cubicles were designed and manufactured by Bastogne Manufacturing, LLC.

The full-scale blast cubicle was tested at the Hurricane Test Laboratory (HTL) in Lubbock, Texas. HTL tested three identical blast cubicles for Bastogne Manufacturing under a full scale blast. Each of the cubicles was tested for the same explosive weight of 50lb TNT and standoff distances of 20, 25, and 30ft as shown in Figure 4-3. The explosive was detonated on the ground surface.

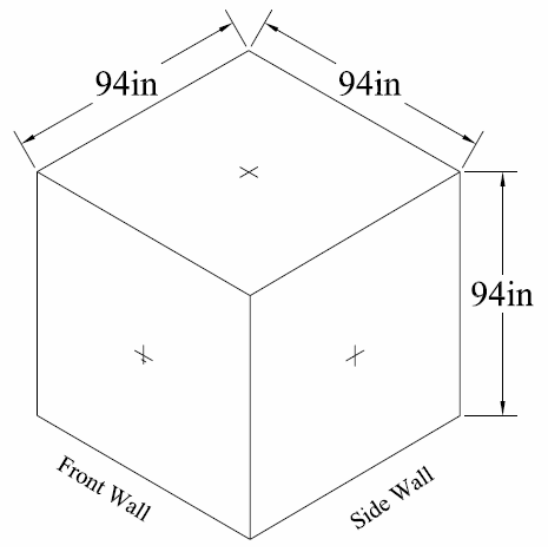

Figure 4-1 Blast cubicle outside dimensions

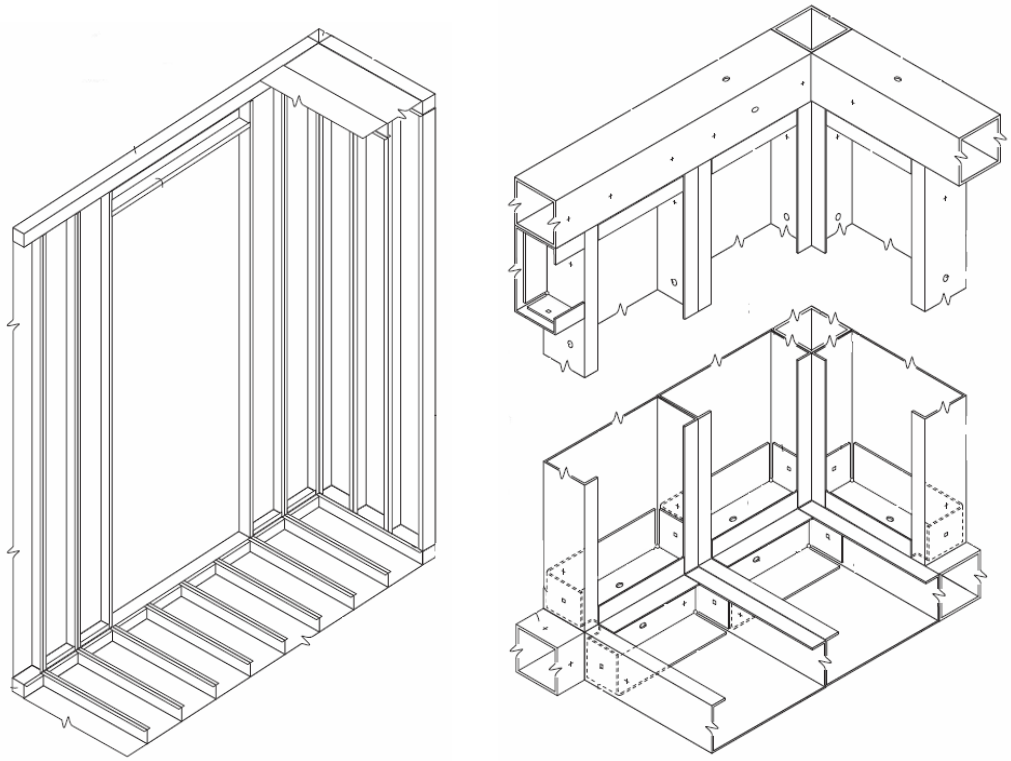

Figure 4-2 Typical blast cubicle frame and channel construction

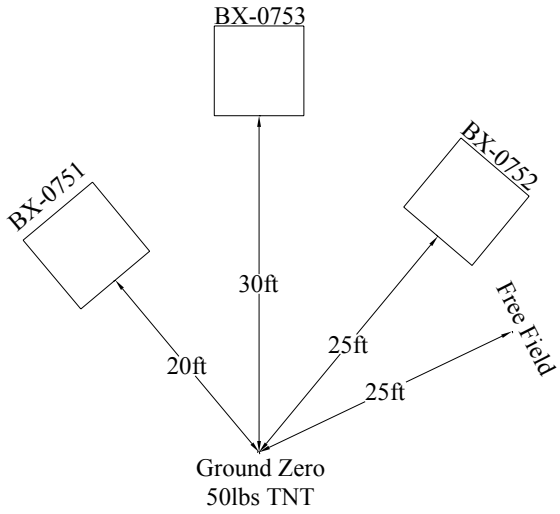

Figure 4-3 Site Plan

HTL used a high speed data acquisition system with a system record time of one-hundred thousand samples per second. Three pressure transducers (PTs) were placed on each blast cubicle with one in the geometric center of the front face, side face, and roof to measure the pressure time history. A separate PT was placed in the free field at a distance of 25ft from the blast to measure the free field pressure time history. The free field PT was approximately four feet above the ground, the same as the PTs placed on the front wall of the blast cubicles. One accelerometer, mounted 2 inches below the PT, measured the acceleration time history on each front wall. Locations of the PTs and accelerometer are shown in Figure 4-4. To validate the accelerometer reading a dryer vent was placed at the inside geometric center of the front wall to measure the maximum relative deflection of the wall to the floor as shown in Figure 4-5. After the blast the deflection of the dryer vent was measured by hand and gave an approximate deflection value for the front wall.

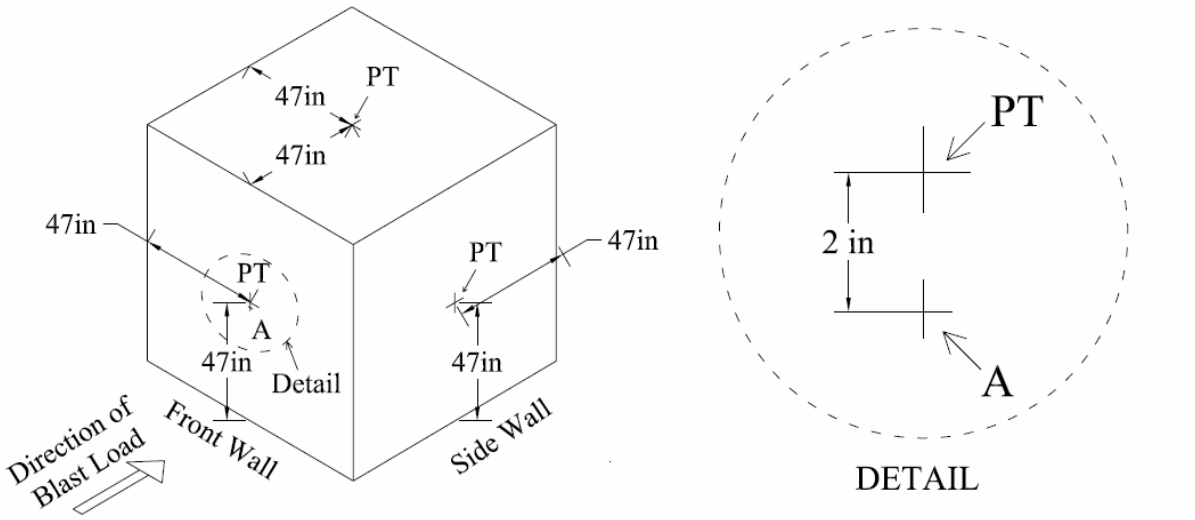

Figure 4-4 Locations of PTs and accelerometer



Figure 4-5 Dryer Vent Deflection Indicator

4.3 Experimental and Theoretical Results

A surface blast test was conducted simultaneously for three blast cubicles, each with a different standoff distance of 20, 25, and 30ft. The purpose of the test was to determine the blast resistant capabilities of the cubicle. The results of the pressure time history were compared to a theoretical analysis using *Structures to Resist the Effects of Accidental Explosions, Army TM 5-1300.* In addition, the front wall pressure transducer and accelerometer readings were compared to results from SDOF, an analysis program provided by the General Services Administration (GSA). Bastogne Manufacturing provided the SDOF results. A second SDOF analysis was conducted using Newmark-β numerical integration to calculate deflection, velocity, and acceleration.

The roof pressure transducers returned unreasonable pressure results after the initial positive pressure due to extreme upward deflection as the blast wave passed. Therefore, no comparison was made between the roof pressure time curves and TM 5-1300. The total load durations for the experimental field tests were determined from the pressure time curves and taken at the completion of the negative pressure phase where the pressure returned to zero and leveled off. Small positive or negative pressures after the negative pressure phase were not considered part of the total load duration. A summary of the test results for maximum positive pressure, maximum negative pressure, positive impulse, positive load duration, and total load duration for the front and side faces are listed in Tables 4-1 and 4-2. The maximum positive pressure for the roof is in Table 4-3. The accelerometer only recorded acceleration versus time. The acceleration data was integrated to obtain the velocity and subsequently integrated to find the deflection. The

Table 4-1 Pressure-time history values for the front face

Specimen	BX-0751 @ 20ft			BX-0752 @ 25ft			BX-0752 @ 30ft			Free field @ 25ft	
	E	T	SDOF	E	T	SDOF	E	T	SDOF	E	T
P_r [a] (psi)	98.9	110	122.8	51	63	64.4	33	35	39.5	18.1	14.4
P_r^- [b] (psi)	-12.9	-5.8	-5.6	-7.6	-4.2	-4.2	-5.3	-3.6	-3.4	-3.3	-7.6
i_r [c], (psi-ms)	73.5	128.9	136.2	68.6	103.2	104.4	50.1	81.1	84.6	27.3	29.2
t_o [d] (msec)	3.4	2.3	2.2	4.1	2.8	3.2	4.3	4.6	4.3	5.9	4.1
t_{total} [e] (msec)	39.1	39.3	39.3	36.1	29.8	40.7	36.1	37.1	42	44.5	45.3

E: pressure transducer experimental, T: TM 5-1300 theoretical, SDOF: single degree of freedom theoretical
[a] maximum positive pressure
[b] maximum negative pressure
[c] positive impulse
[d] positive load duration
[e] total load duration

Table 4-2 Pressure-time history values for the side face

Specimen	BX-0751 @ 20ft		BX-0752 @ 25ft		BX-0752 @ 30ft	
	E	T	E	T	E	T
P_r [a] (psi)	22.8	17	16.2	14.4	8.4	8.3
P_r^- [b],(psi)	-3.5	-9.4	-3.3	-7.6	-3.4	-3.6
i_r [c], (psi-ms)	24.5	29.8	20.9	29.2	16.9	22.8
t_o [d] (msec)	7.5	5.5	4.7	4.1	5.2	5.5
t_{total} [e] (msec)	41	46.8	46.3	45.3	45.1	44.2

E: pressure transducer experimental, T: TM 5-1300 theoretical, SDOF: single degree of freedom theoretical
[a] maximum positive pressure
[b] maximum negative pressure
[c] positive impulse
[d] positive load duration
[e] total load duration

Table 4-3 Pressure-time history experimental values for roof

Specimen	BX-0751 @ 20ft		BX-0752 @ 25ft		BX-0752 @ 30ft	
	E	T	E	T	E	T
P_r [a] (psi)	20.5	17	16.7	14.4	11.9	8.3
P_r^- [b],(psi)	N/A	-9.4	N/A	-7.6	N/A	-3.6
i_r [c], (psi-ms)	N/A	29.8	N/A	29.2	N/A	22.8
t_o [d] (msec)	N/A	5.5	N/A	4.1	N/A	5.5
t_{total} [e] (msec)	N/A	46.8	N/A	45.3	N/A	44.2

E: pressure transducer experimental, T: TM 5-1300 theoretical, DC: data corrupted
[a] maximum positive pressure
[b] maximum negative pressure
[c] positive impulse
[d] positive load duration
[e] total load duration

accelerometer data was then filtered in Matlab using high and low pass filters. A Fast Fourier Transform (FFT) converted the data from time domain to frequency domain and determined the natural frequency to be 24Hz. The frequency range was from zero to 50,000Hz. Thus the high pass filter was set at 15Hz and the low pass filter at 3000Hz.

The Newmark-β linear analysis used a β value of 1/6 and a damping ratio of 4.37%, as obtained from test results performed by Bastogne Manufacturing on a section of the wall. The Newmark-β method used a natural frequency of 30Hz as obtained from the wall section calculations included in the Appendix. The theoretical pressure-time history from TM5-1300 (1990) was applied to determine the theoretical deflection, velocity, and acceleration with a sample rate of one-hundred thousand samples per second.

4.3.1 Blast cubicle BX-0751 @ 20ft standoff distance

The front, side, and roof pressure time histories are shown in Figures 4-6, 4-7, and 4-8. The values for the maximum and minimum pressure, positive impulse, and positive and total load durations for the front and side walls are listed in Tables 4-1 and 4-2. The maximum positive pressure for the roof is in Table 4-3.

The front face pressure loading from the experimental readings generally fit the form of an ideal blast curve. However there were two sharp pressure spikes in the positive phase loading. The negative phase also experienced abnormal readings increasing sharply to positive values twice before the end of the negative phase. The theoretical positive impulse for the front face was 43% larger than the experimental impulse.

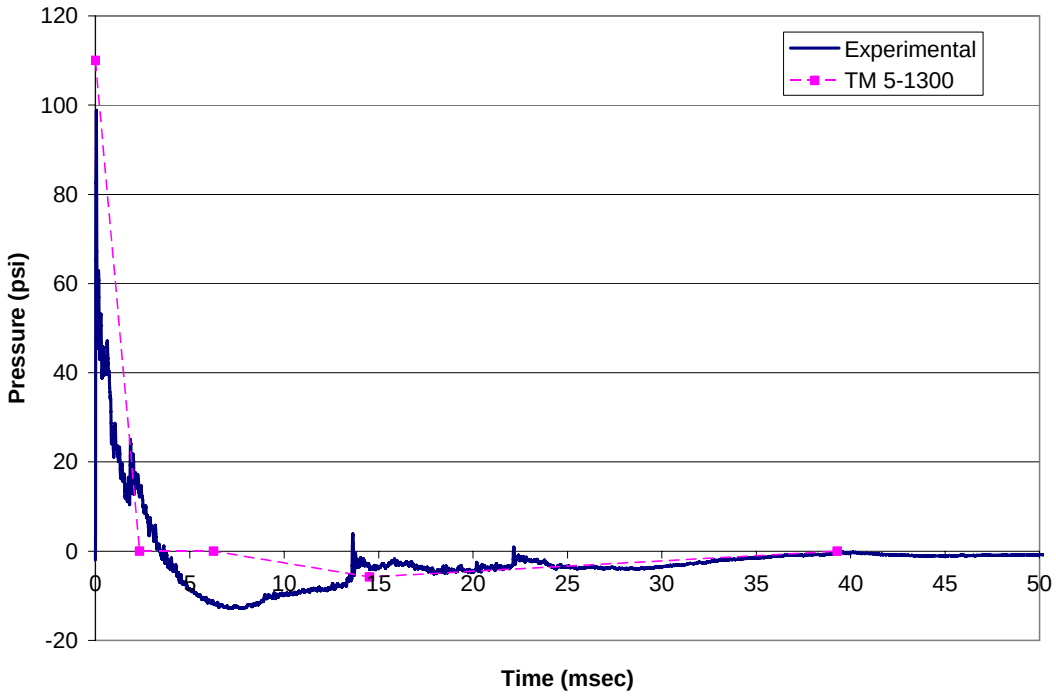

Figure 4-6 Air Blast Pressure Time History BX-0751 Front Wall (20ft standoff distance)

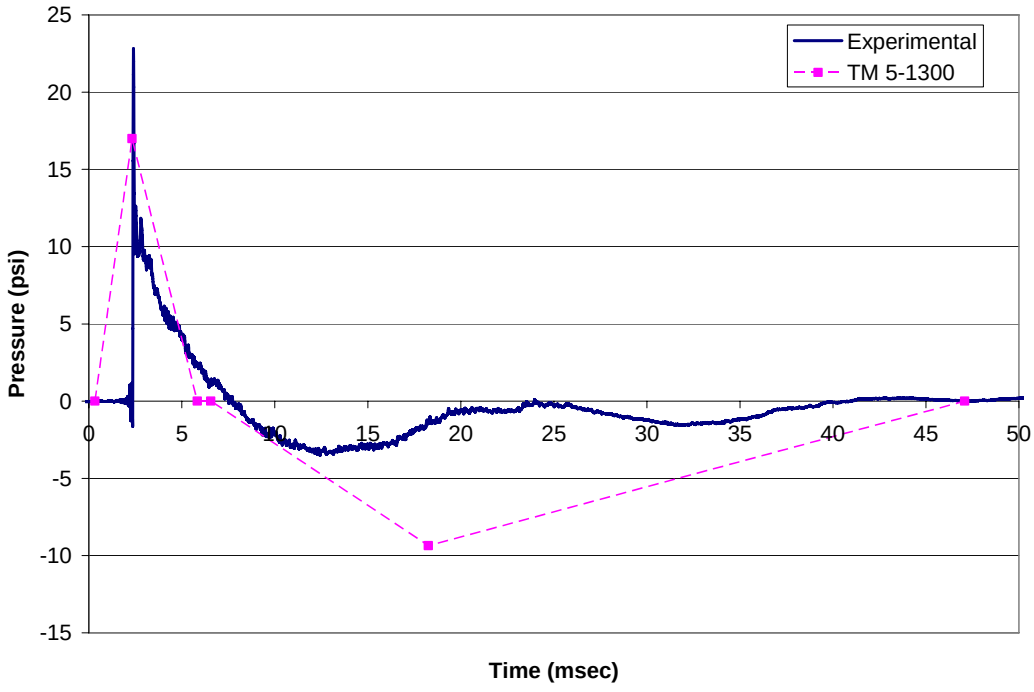

Figure 4-7 Air Blast Pressure Time History BX-0751 Side Wall (20ft standoff distance)

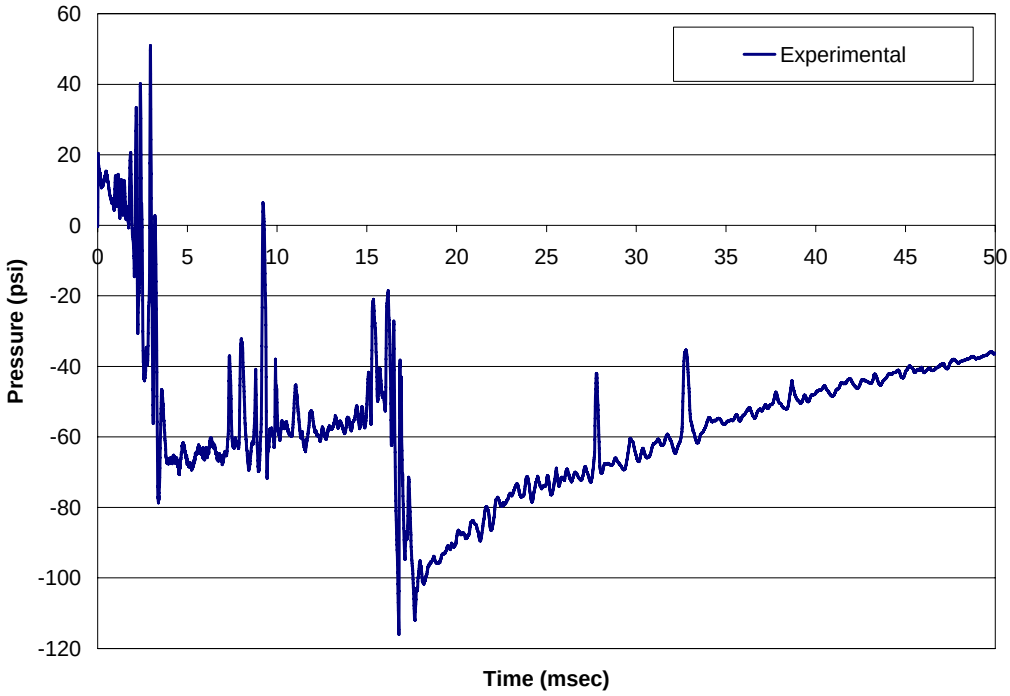

Figure 4-8 Air Blast Pressure Time History BX-0751 Roof (20ft standoff distance)

The side face experimental loading was a smooth pressure-time curve throughout the positive phase. There is a time lag from the start of the reading to the arrival of the positive pressure loading, possibly because the reading was started when the blast wave first struck the front face of the cubicle. The negative phase exhibits variations by rising slightly before dropping and then leveling out at the ambient pressure. The theoretical maximum positive pressure was less than the experimental positive pressure but the theoretical positive impulse for the side face was 17.8% larger than the experimental impulse. The theoretical negative pressure was over twice the experimental negative pressure and not an accurate approximation.

The maximum and minimum values of acceleration, velocity, and deflection from the accelerometer, SDOF, and Newmark-β method are listed in Table 4-4. The acceleration, velocity, and deflection time histories are shown in Figures 4-9, 4-10, and 4-11.

The front and side walls exhibited elastic behavior with no visible permanent deformation observed after the blast. However, the roof had an upward inelastic deformation with a hand-measured maximum deflection of 4.5 in. The SDOF acceleration was over five times as great as the experimental value and the velocity over ten times as great as the experimental velocity. However, the SDOF deflection was on the same order of magnitude as the experimental result, though slightly larger. The Newmark-β method underestimated the deflection and was only half of the experimental value and the velocity was only slightly greater than half of the experimental velocity value. The acceleration was greatly underestimated and was not comparable to the experimental value as it was over ten times smaller.

Table 4-4 Front face accelerometer results

Specimen		BX-0751 @ 20ft				BX-0752 @ 25ft				BX-0753 @ 30ft	
		Original	Filtered	SDOF	Newmark-Beta	Original	Filtered	SDOF	Newmark-Beta	SDOF	Newmark-Beta
Acceleration (g)	max	568.1	529.4	3509.3	57.4	275.5	270.4	1835.4	39.2	1127.3	33.9
	min	-486.9	-452	-484.4	-37.8	-188.9	-190.2	-375.8	-23.4	307.1	-24.1
Velocity (in/s)	max	140.8	139.3	1464	68.9	77.9	75.8	1134	41.7	943.2	39.3
	min	-110.2	-69.9	-1488	-69.4	-91.2	-100.9	-1164	-42.7	-961.2	-44.1
Deflection (in)	max	0.99	1.14	1.09	0.39	0.59	0.55	0.859	0.21	0.714	0.21
	min	-0.392	0	-1.28	-0.34	-0.566	-0.864	-0.986	-0.19	-0.0819	-0.18

SDOF: single degree of freedom theoretical

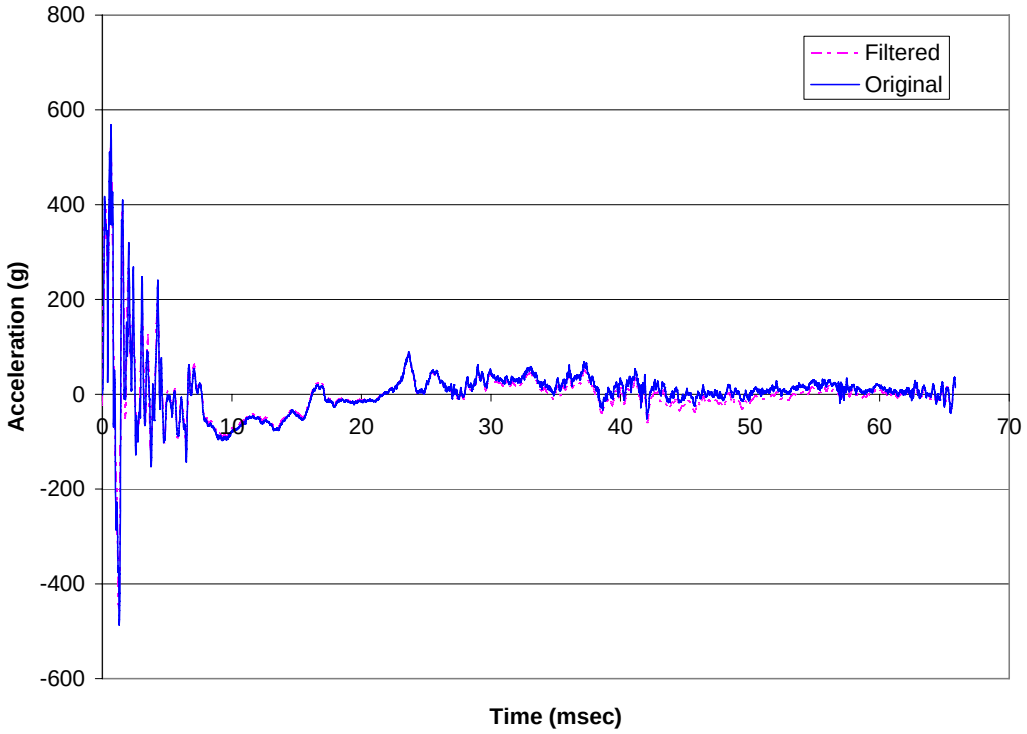

Figure 4-9 Acceleration Time History BX-0751 Front Wall

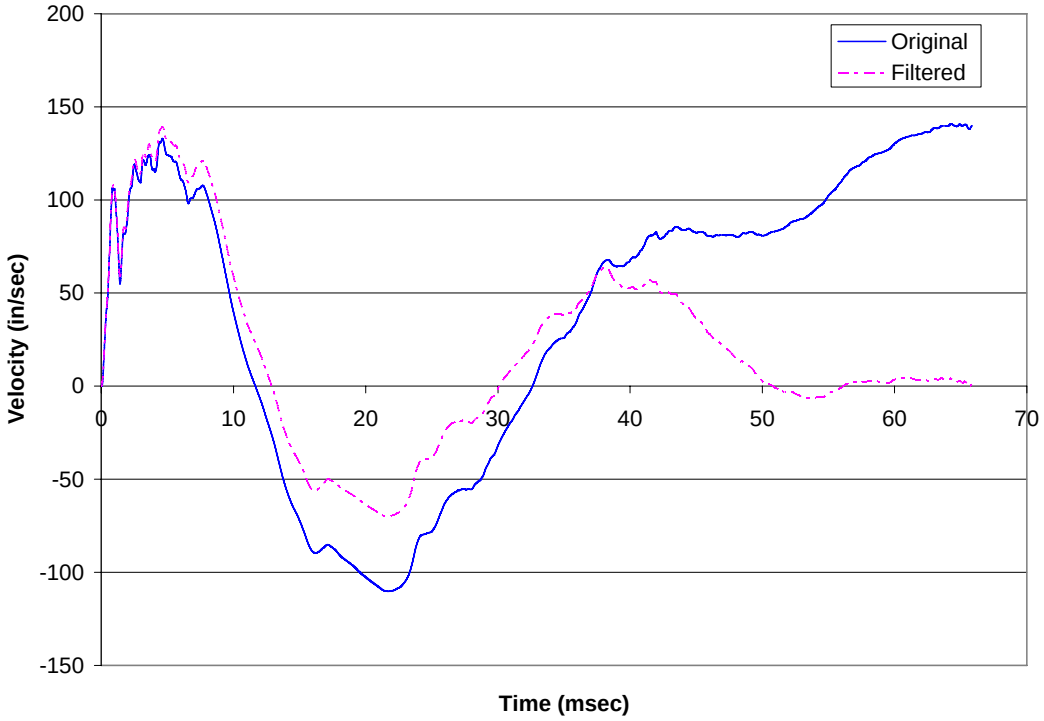

Figure 4-10 Velocity Time History BX-0751 Front Wall

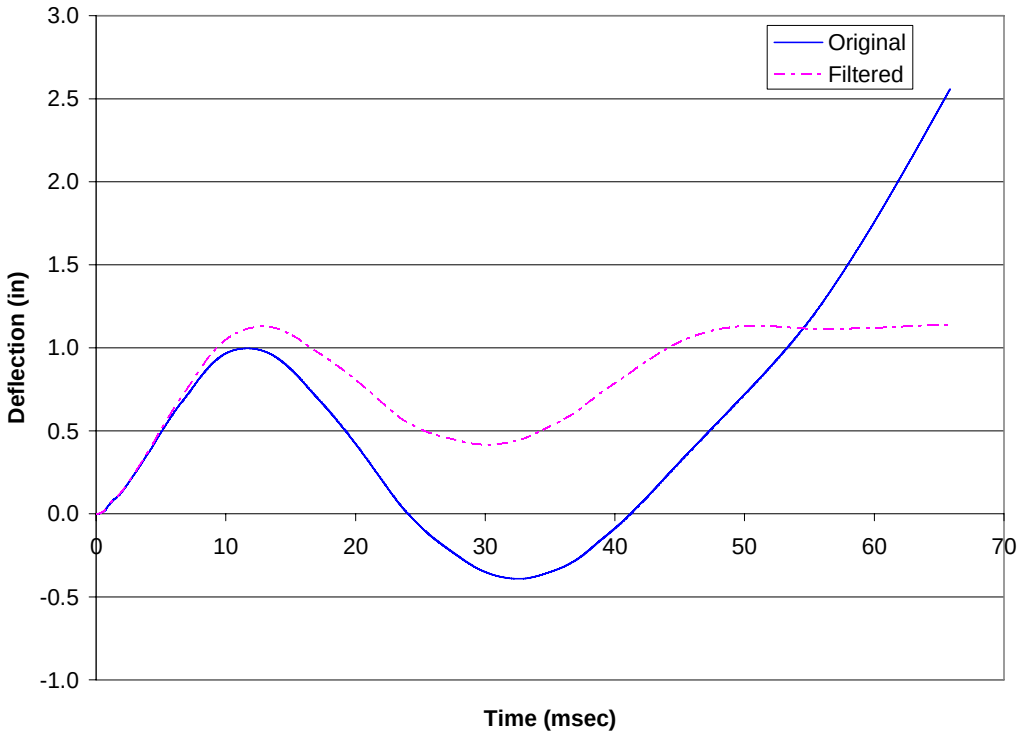

Figure 4-11 Deflection Time History BX-0751 Front Wall

4.3.2 Specimen BX-0752 @ 25ft standoff distance

The front, side, and roof pressure time histories are shown in Figures 4-12, 4-13, and 4-14. The values for the maximum and minimum pressure, positive impulse, and positive and total load durations for the front and side walls are listed in Tables 4-1 and 4-2. The maximum experimental positive pressure for the roof is in Table 4-3.

The experimental results for the front face returned a smooth pressure time curve in the positive phase. There was one discrepancy in the positive phase region with an abnormal drop in the pressure before returning to the ideal blast curve. The negative phase had an abnormal jump into the positive pressure region before returning to the ambient pressure. The theoretical positive impulse was 33.5% larger than the experimental impulse.

The side face experimental positive phase curve was smooth, but the negative phase had jumps of pressure uncharacteristic of a blast pressure time curve. The maximum theoretical negative pressure was twice the maximum experimental negative pressure and was overly conservative. The theoretical positive impulse for the side face of BX-0752 was 28.4% larger than the experimental impulse.

The maximum and minimum values of acceleration, velocity, and deflection from the accelerometer, SDOF, and Newmark-β method are listed in Table 4-4. The acceleration, velocity, and deflection time histories are shown in Figures 4-15, 4-16, and 4-17.

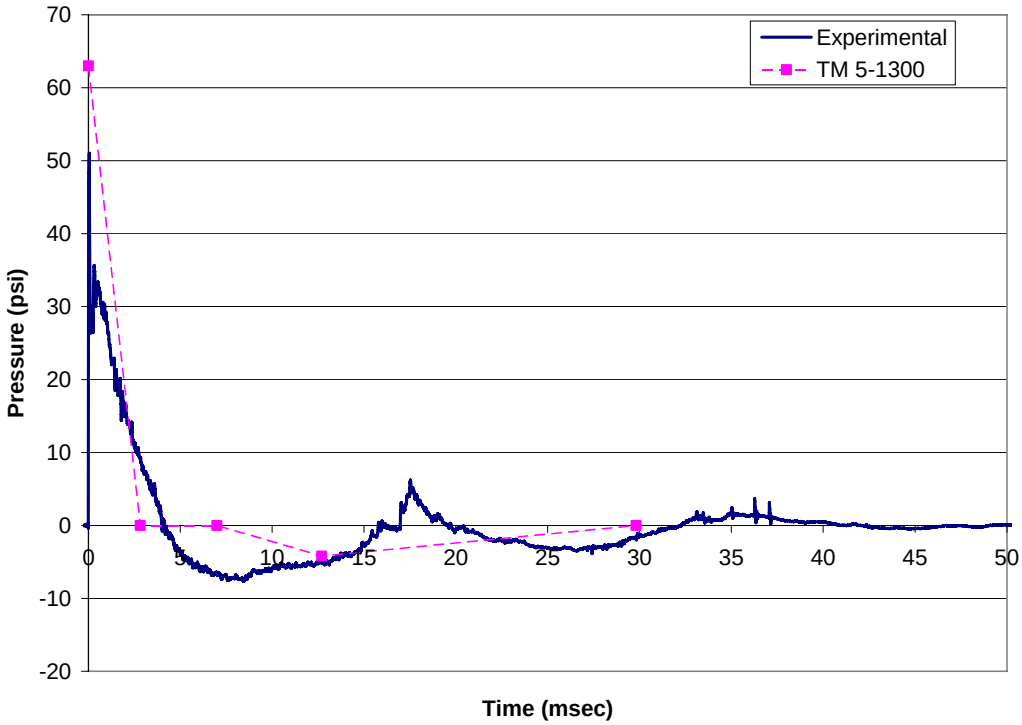

Figure 4-12 Air Blast Pressure Time History BX-0752 Front Wall (25ft standoff distance)

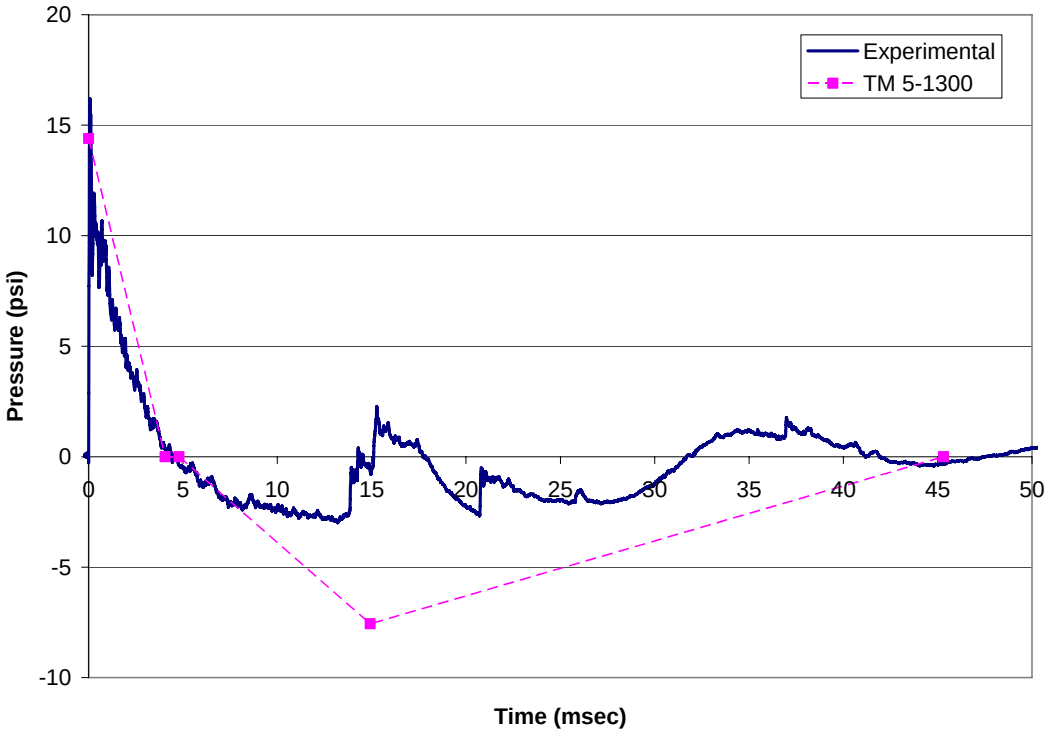

Figure 4-13 Air Blast Pressure Time History BX-0752 Side Wall (25ft standoff distance)

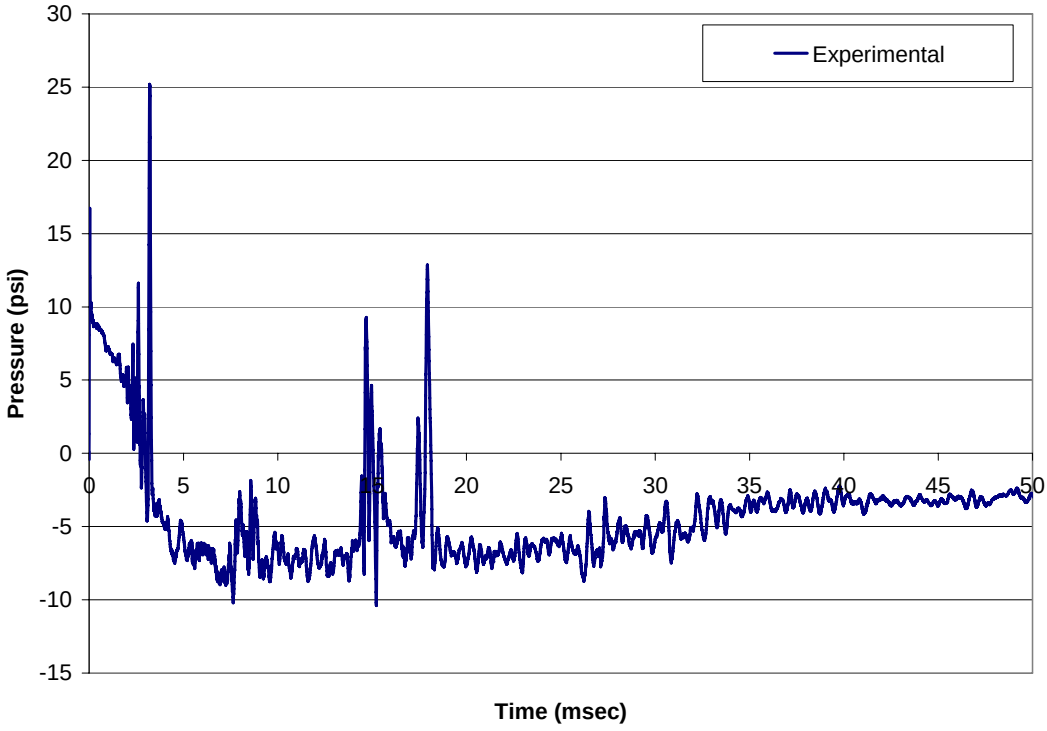

Figure 4-14 Air Blast Pressure Time History BX-0752 Roof (25ft standoff distance)

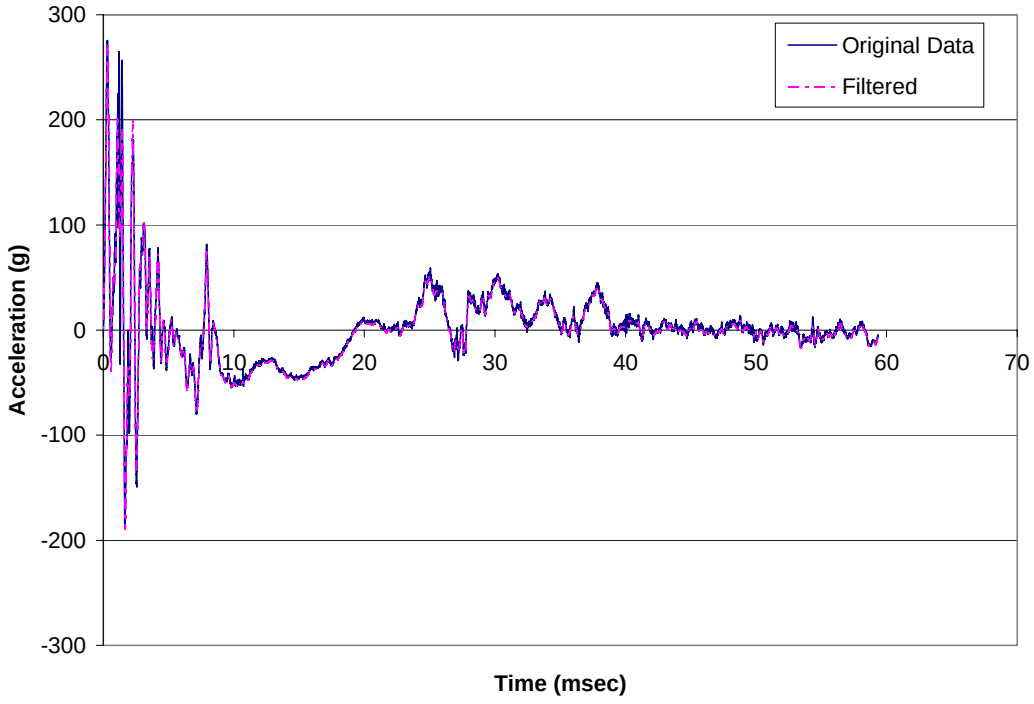

Figure 4-15 Acceleration Time History BX-0752 Front Wall

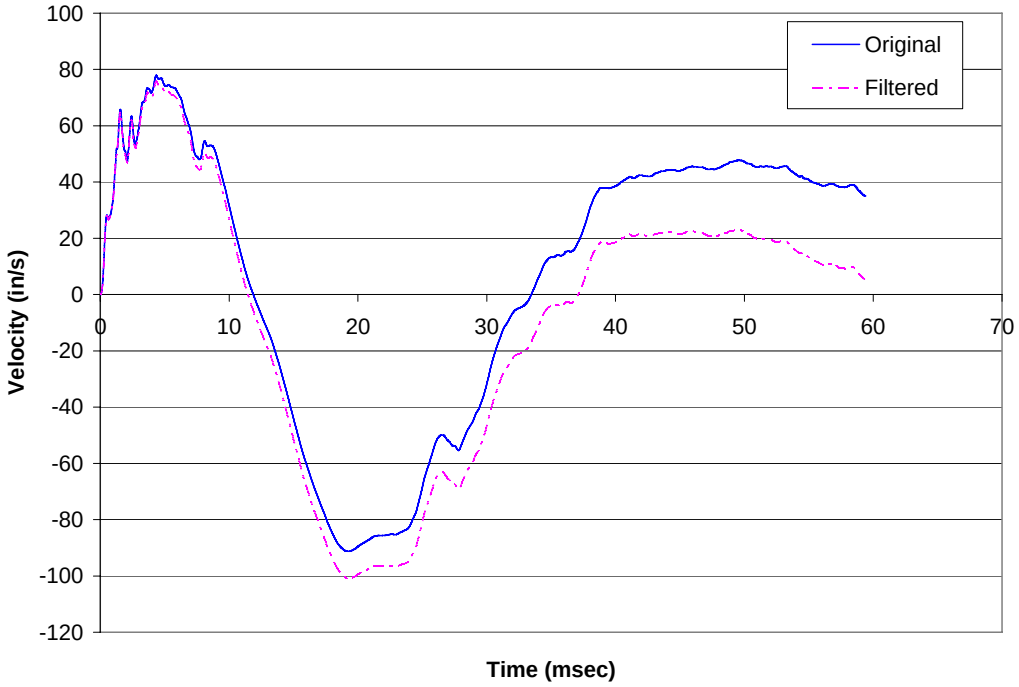

Figure 4-16 Velocity Time History BX-0752 Front Wall

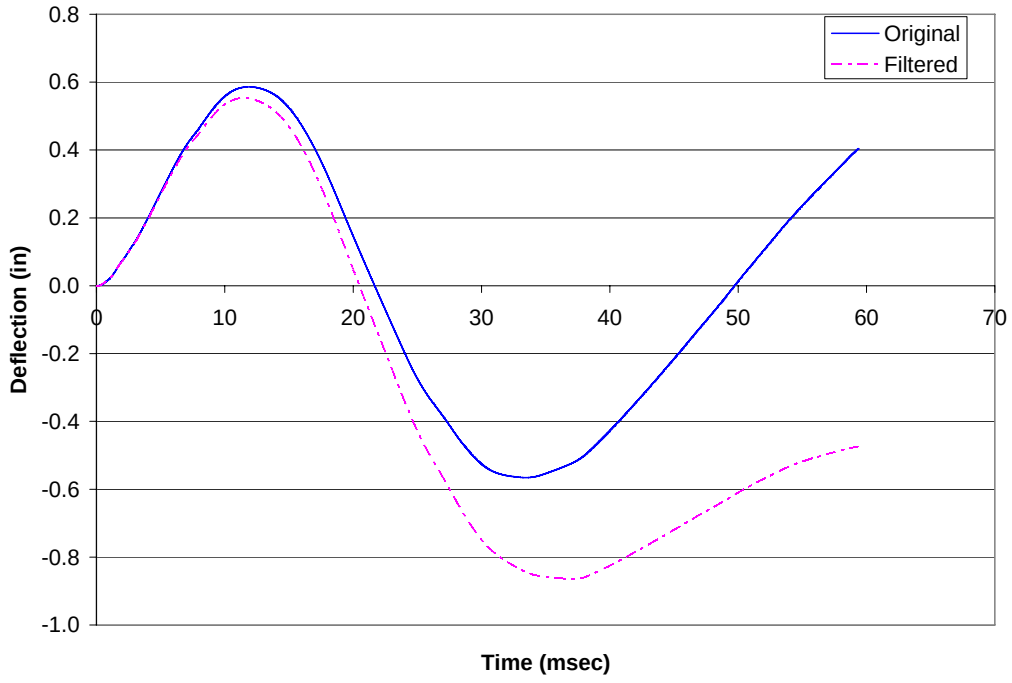

Figure 4-17 Deflection Time History BX-0752 Front Wall

The front and side walls exhibited elastic behavior with no visible permanent deformation observed after the blast. However, the roof had an upward inelastic deformation with a hand measured maximum deflection of 4.25 in. The SDOF acceleration was over five times and the velocity over ten times as great as the experimental values. The SDOF deflection was on the same order of magnitude and slightly larger than the experimental result. The Newmark-β method underestimated the deflection and was only half of the experimental value and the velocity was only slightly greater than half of the experimental velocity value. The acceleration was greatly underestimated and was over ten times smaller than the experimental value.

4.3.3 Specimen BX-0753 @ 30ft standoff distance

The front, side, and roof pressure time histories are shown in Figures 4-18, 4-19, and 4-20. The values for the maximum and minimum pressure, positive impulse, and positive and total load durations for the front and side walls are listed in Tables 4-1 and 4-2. The maximum experimental positive pressure for the roof is in Table 4-3.

The front face had a smooth positive phase curve but experienced jumps in the data in the negative loading phase. The theoretical positive impulse for the front face was 38.2% larger than the experimental impulse.

The side face experimental positive phase was a smooth curve, but the negative phase experienced many jumps in the pressure loading. Though slightly unconservative, the theoretical maximum positive pressure closely predicted the maximum positive experimental pressure. The theoretical positive impulse for the side face was 25.9%

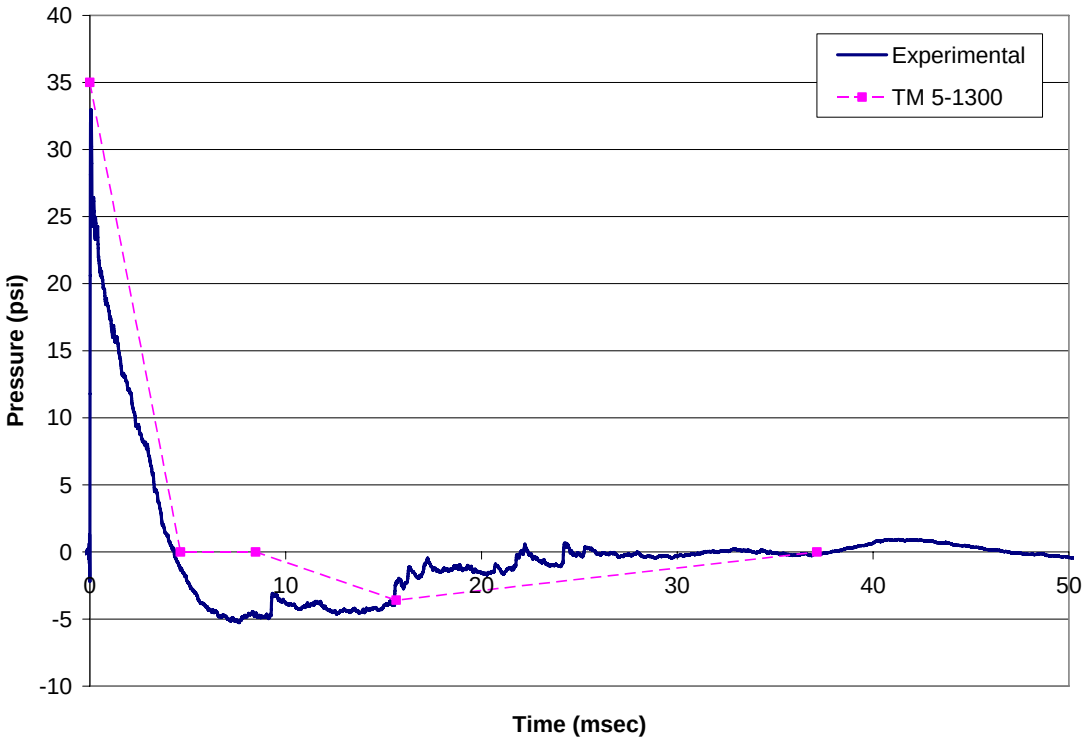

Figure 4-18 Air Blast Pressure Time History BX-0753 Front Wall (30ft standoff distance)

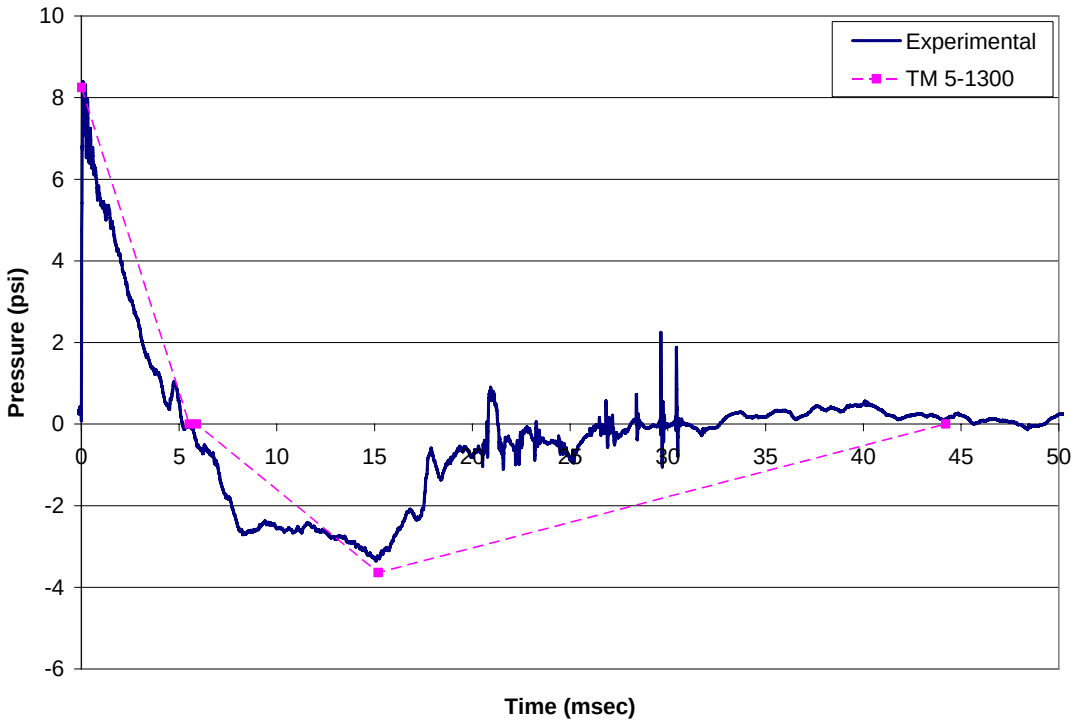

Figure 4-19 Air Blast Pressure Time History BX-0753 Side Wall (30ft standoff distance)

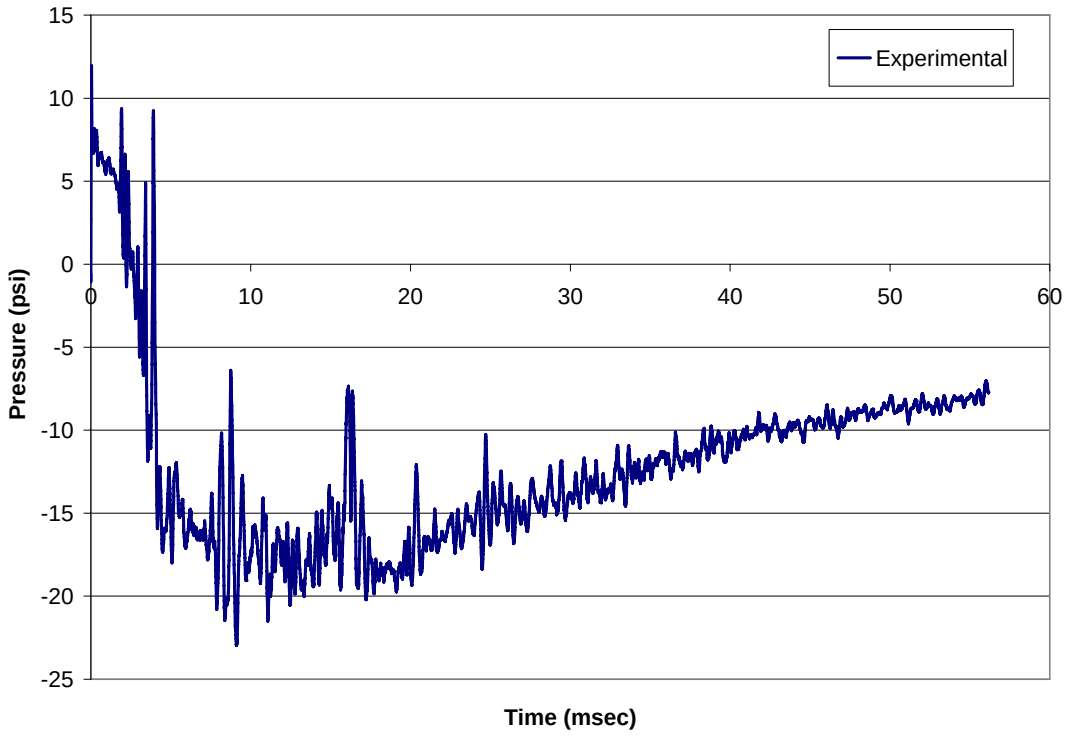

Figure 4-20 Air Blast Pressure Time History BX-0753 Roof (30ft standoff distance)

larger than the experimental impulse. HTL did not provide the acceleration, velocity, and deflection time histories due to an instrumentation failure that returned invalid results.

The front and side walls showed elastic behavior with no visible permanent deformation observed after the blast. However, the roof had an upward inelastic deformation with a hand measured maximum deflection of 3.5 in. The maximum and minimum values of acceleration, velocity, and deflection from the SDOF and Newmark-β method are listed in Table 4-4.

The front and side walls exhibited elastic behavior with no visible permanent deformation observed after the blast. However, the roof had an upward inelastic deformation with a hand-measured maximum deflection of 4.5 in.

4.3.4 Free Field Surface Burst

A free field pressure transducer was placed at 25ft from the center of the 50lb TNT explosive. It was at a height of approximately 4ft above the ground surface. The graph for the pressure time history is shown in Figure 4-21. The values for the maximum and minimum pressure, positive impulse, and positive and total load durations are listed in Table 4-1.

The free field pressure transducer was located 25ft from the explosive. Therefore the pressure time curve results should have been similar to those experienced by the front face of cubicle BX-0752. The free field pressure curve did not return results as expected but rather a curve similar to the side face loading on BX-0752. The reason for this discrepancy was likely due to the following factors. While the measurement was stated as being free field, in the blast test the pressure transducer was actually located next to

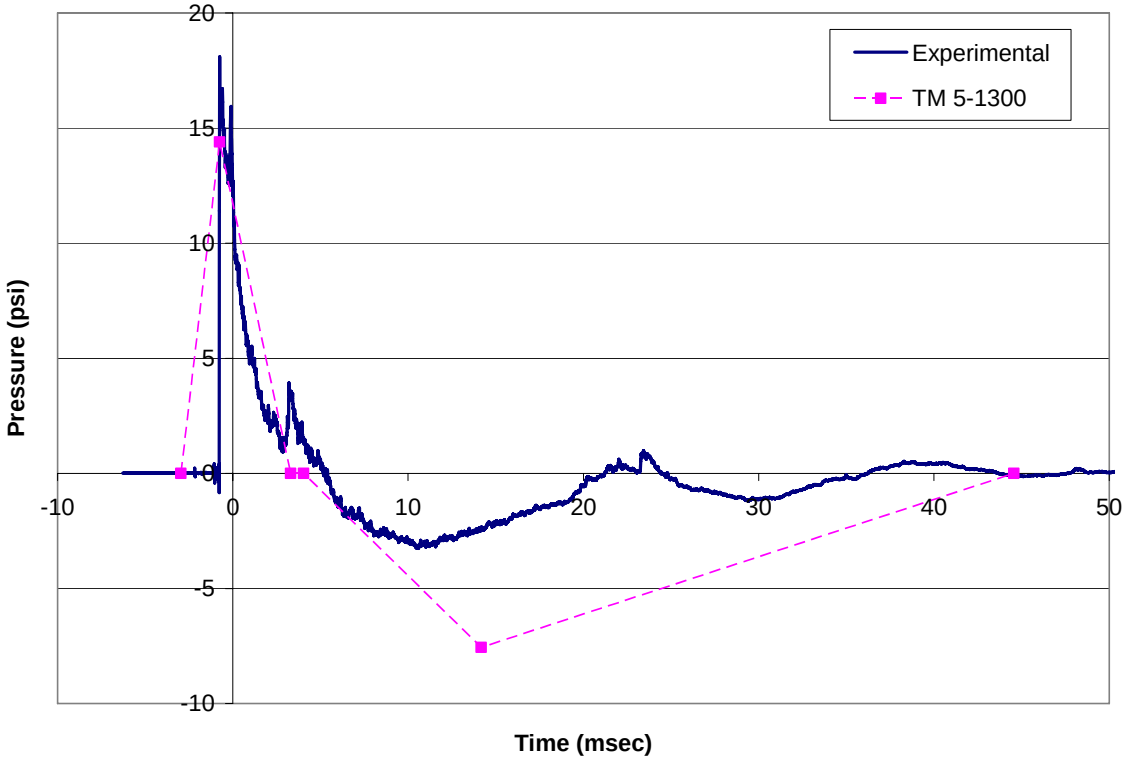

Figure 4-21 Free Field Surface Burst at 25ft

blast cubicle BX-0752. To have an actual free field measurement the transducer should have been located in the open by itself. Also the pressure transducer was not oriented toward the blast, but situated at a 90° angle from the blast front. This likely explains the pressure time curve being similar to the side face loading of BX-0752 instead of the front face loading.

The experimental reading is a typical pressure time curve with only one spike of pressure in the positive pressure phase. However, the positive pressure data began at -0.75msec which brings into doubt when the pressure transducer began recording the blast wave. It is assumed the initial positive pressure reading was the point at which the blast wave struck the pressure transducer. The results were compared to the theoretical side loading on BX-0752. The theoretical maximum positive pressure was less than the experimental value but the correlation between the positive impulses was excellent with the theoretical impulse only 6.9% larger than the experimental impulse. The theoretical negative phase loading was inaccurate with a maximum negative value that was twice that measured during the testing.

4.3.5 Dynamic Properties

Multiple free-vibration tests were conducted by Bastogne Manufacturing to determine the damping ratio for a specimen that was a sub-assembly of the blast cubicle wall panel. The specimen consisted of one channel, a wall plate on one side, and end plates and then was filled with sand. During the test, the specimen was laid horizontally and clamped at the ends. A magnet was used to apply an initial upward deflection and held the wall at rest prior to the test initiation. At test initiation the magnet was removed,

thus causing the free vibration of the specimen. One accelerometer was placed at the mid-span of the specimen to record the acceleration versus time data. Tests were conducted on the specimen for two scenarios: specimen filled with sand and specimen without sand. The experimental test setup is shown in Figure 4-22.

The test data was analyzed at the University of Tennessee in order to determine damping ratios and natural periods with the method outlined in Lu and Silva (2006), and the results are given in Table 4-5. From the results, it is obvious that with addition of sand, the damping ratio did not significantly change with less than of 50% increase. However, the natural frequency was greatly decreased with the sand addition, which helps in decreasing the impulsive load. The results from test-1-with-sand were used for the SDOF software analysis performed by Bastogne Manufacturing.



Figure 4-22 Wall section free vibration test setup

Table 4-5 Wall section free vibration test results

	Damping Ratio (%)	T_n (sec)	ω_n (rad/sec)	f_n(Hz)
Test 1 with sand	4.37	.06107	102.88	16.37
Test 3 with sand	5.25	.06098	103.04	16.40
Test 4 with sand	5.57	.06121	102.66	16.34
Test 5 with sand	5.92	.06142	102.29	16.28
Test 1 without sand	3.55	.03184	197.33	31.41
Test 2 without sand	3.89	.03253	193.14	30.74
Test 5 without sand	3.37	.03235	194.25	30.32

4.4 Discussion of Results

4.4.1 Air Blast Pressure Time History

Both the experimental and the analytical maximum positive pressure at the front face of the three cubicles are shown in Figure 4-23. The experimental and the analytical positive impulse at the front face of the three cubicles are shown in Figure 4-24. From the figures it is obvious that as the stand-off distance of the cubicle increased, the maximum positive pressure and the positive impulse acting on the front surface decreased significantly.

As shown in the figures, the analytical values were always slightly larger than the experimental values, which could be due to several factors. 1) The site surface condition. Prediction of a surface burst assumes that the blast pressure is completely reflected from the ground. For the same explosive weight and standoff distance a perfectly reflected surface burst imparts twice the pressure of a free air burst. The experimental setup was

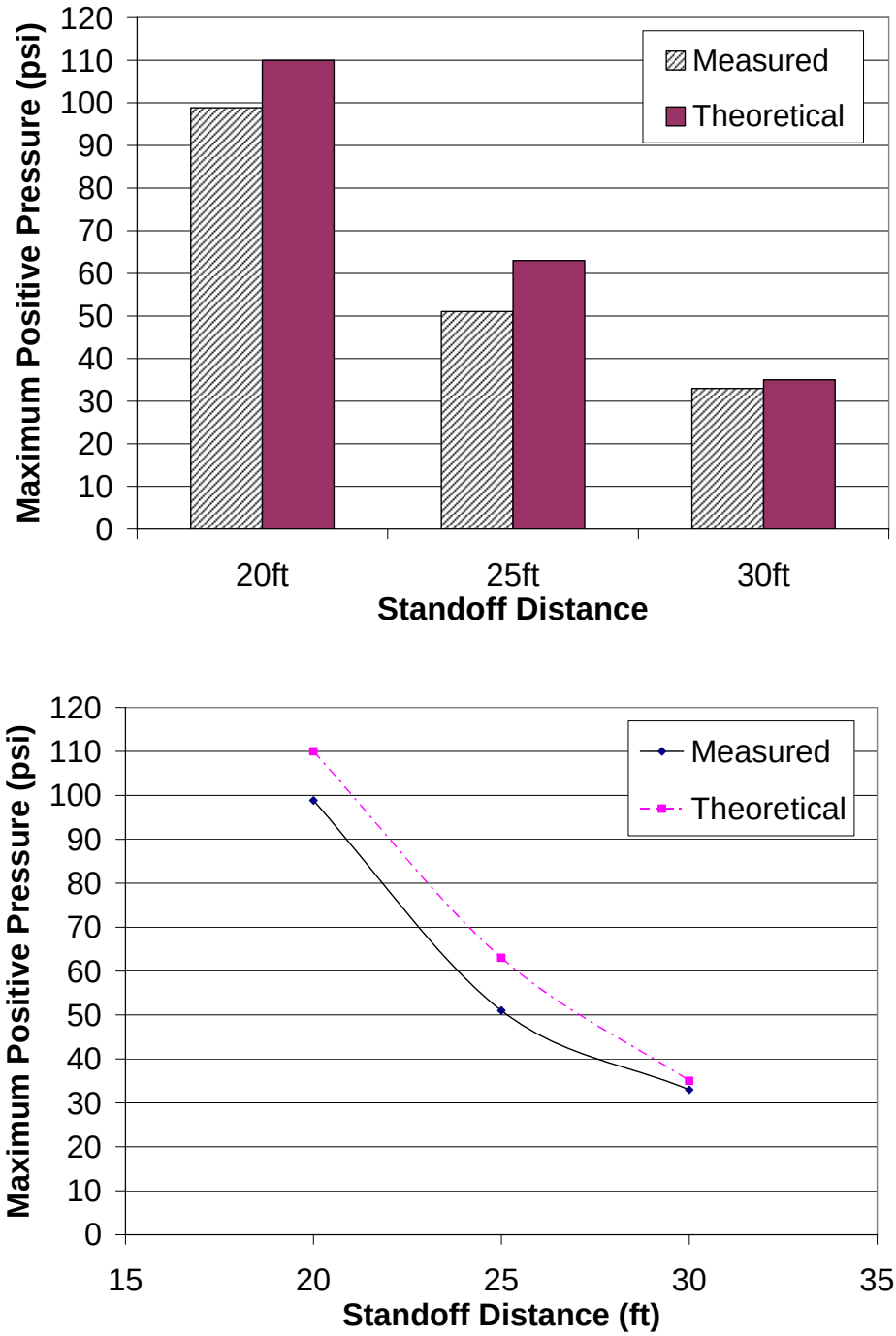

Figure 4-23 Comparison of front face theoretical and experimental maximum positive pressures

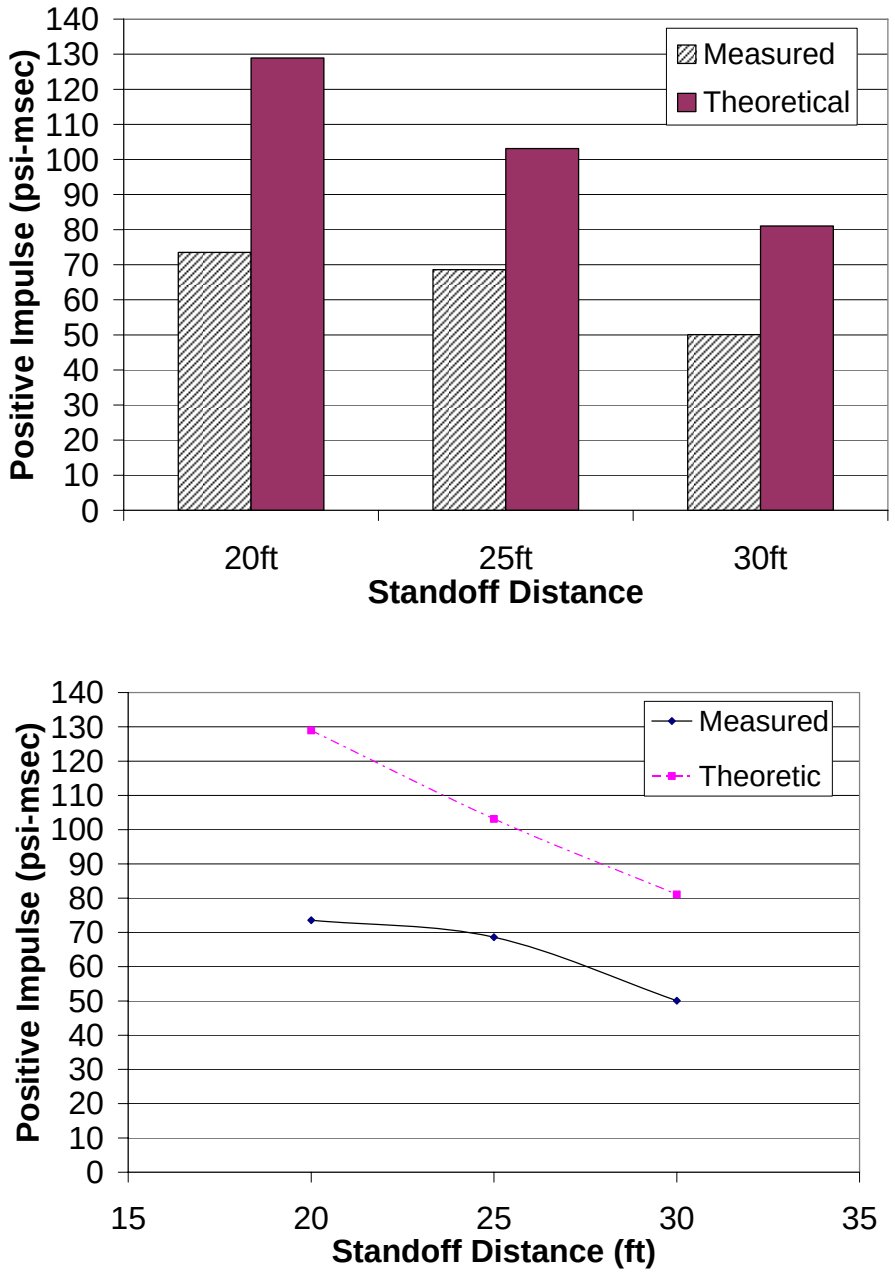

Figure 4-24 Comparison of front face theoretical and experimental positive impulses

conducted on a sandy soil which likely did not return a perfect reflection, indicated by an approximately 11 in deep crater formed after the blast. 2) Absorption of blast energy by the soil. Both factors would result in experimental positive pressure and impulse less than the theoretical values, as shown in Figure 4-23 and Figure 4-24.

For the side face loadings all three blast cubicles exhibited experimental maximum pressure values that were larger than the theoretical maximum pressures as shown in Figure 4-25. However, the experimental positive impulse values were smaller than the theoretical values as shown in Figure 4-26.

For the side faces, TM 5-1300 unconservatively predicted the maximum positive pressures. As the stand-off distance from the blast increased, TM 5-1300 would make a better approximation to the experimental maximum positive pressure values. While the theoretical values for the maximum positive pressures were unconservative, the theoretical values for the positive impulse were conservative, which is more important, since impulses are used to calculate the blast load.

The side face negative maximum pressures were greatly overestimated by TM 5-1300. This value is based on a modification factor which is applied to the maximum positive pressure experienced by the side face. Currently this method does not accurately predict the negative pressure for side face pressure loading. While hardly perfect, TM 5-1300 is reasonable and conservative for prediction of blast loads.

The maximum positive blast pressure and impulse was greatest at the cubicle closest to the blast. As the standoff distance increased the positive blast pressure and impulse decreased for both the front and side walls. A comparison of the front and side

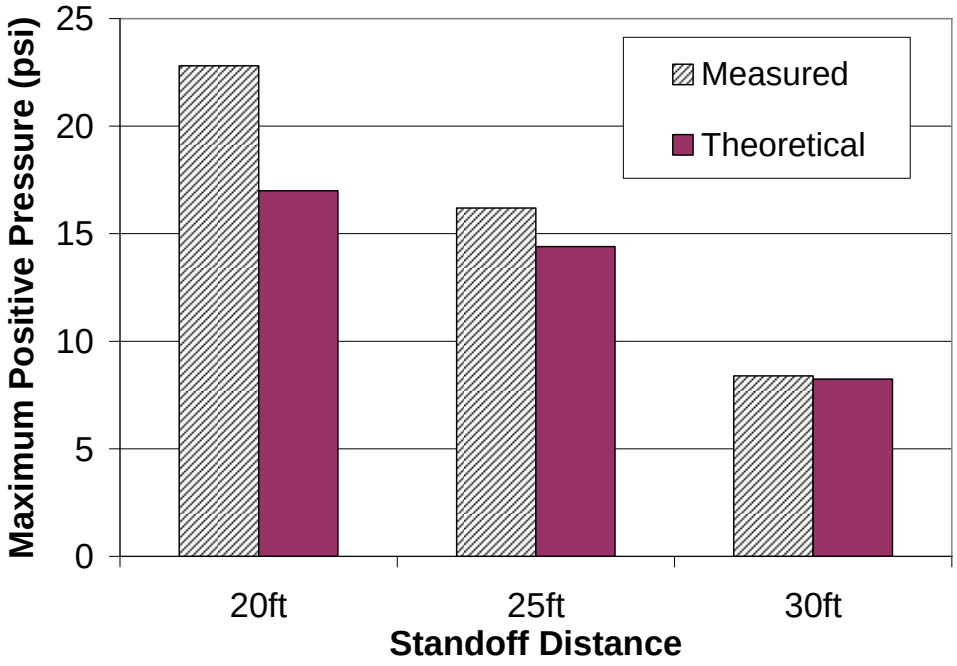

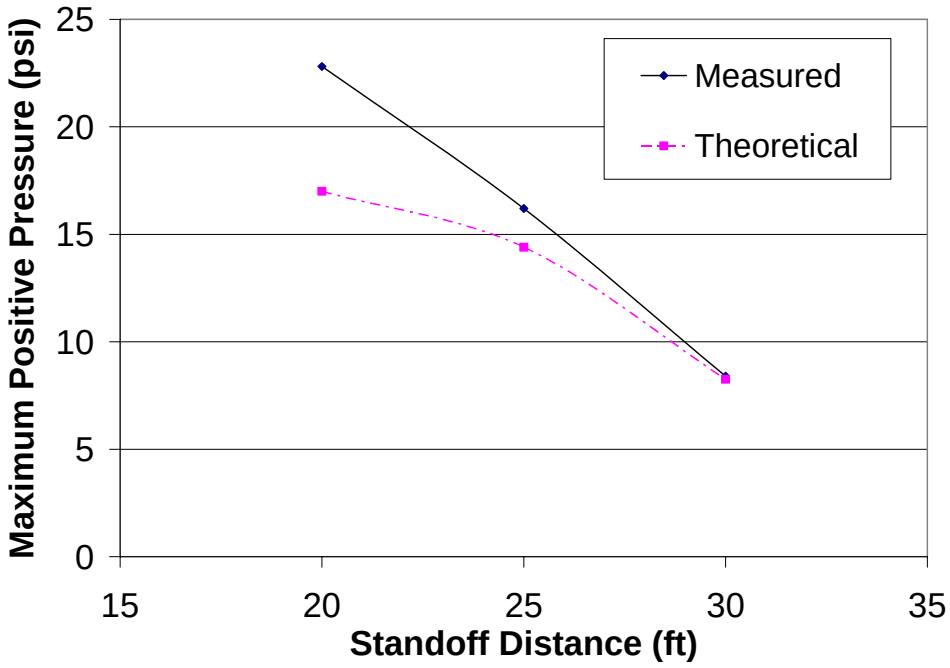

Figure 4-25 Comparison of side face theoretical and experimental maximum positive pressures

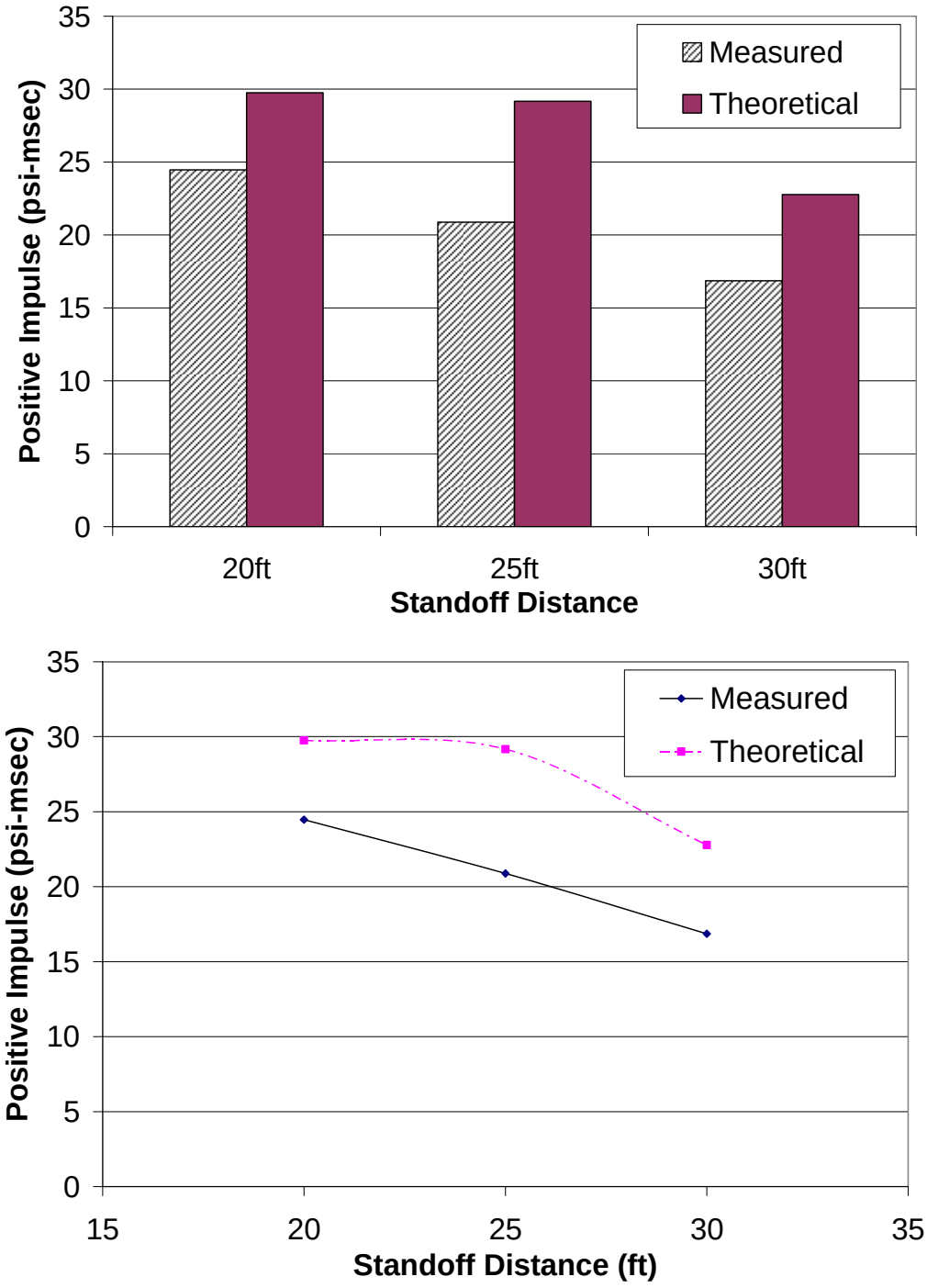

Figure 4-26 Comparison of side face theoretical and experimental positive impulses

face pressure loadings indicates that the front face maximum positive pressures were much greater than the side face maximum positive pressures, as shown in Figure 4-27.

Theoretically, the blast pressure readings on the roof and side walls should be the same. By comparing the initial peak positive pressure for the roofs and the maximum positive pressure for the side walls, a good correlation is seen for cubicles BX-0751 and BX-0752. The correlation is less obvious in cubicle BX-0753, with the roof loading greater than the side face loading, as shown in Table 4-6. No comparison was made between TM 5-1300 and the experimental results due to the invalid data recorded past the initial maximum positive pressure.

4.4.2 Acceleration, Velocity, and Displacement

The acceleration was measured for the front walls of BX-0751 and BX-0752. A dryer vent was used to measure the relative deflection of the front wall to the cubicle floor and validate the accelerometer readings.

Cubicle BX-0751 had an integrated maximum deflection of 2.56 in, first positive peak deflection of 0.99 inches, and the measured dryer vent deflection was 0.81 in. BX-0752 had a maximum integrated deflection of 0.55 in and the dryer vent measured deflection as 0.69 in.

HTL integrated the acceleration time curve using the trapezoidal rule to obtain the velocity, and then integrated the velocity curve again to obtain the displacement curve. While the acceleration data were recorded directly during the blast test, the velocity and displacement values were obtained by the integration process. Therefore, the velocity and

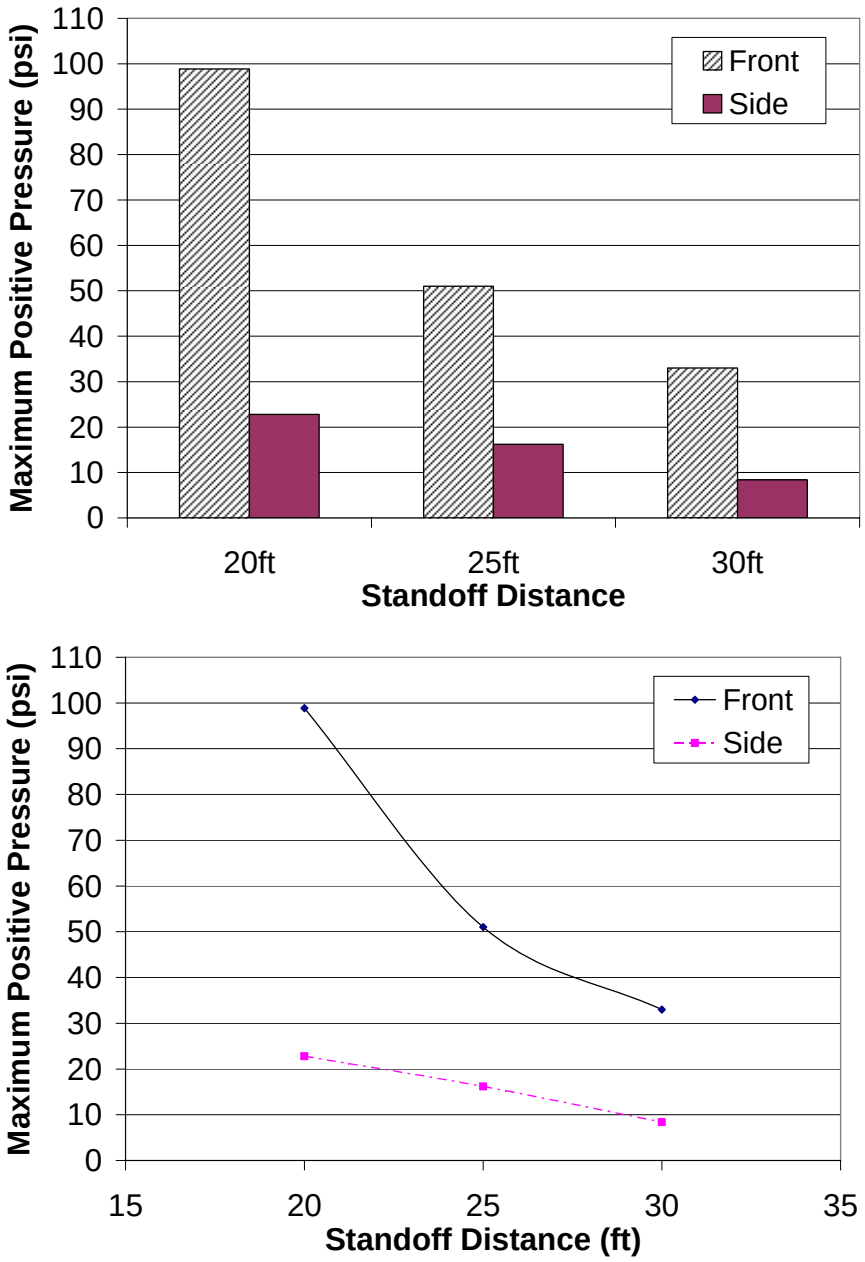

Figure 4-27 Comparison of front and side face experimental maximum positive pressures

Table 4-6 Maximum experimental positive pressure

Specimen	BX-0751 @ 20ft	BX-0752 @ 25ft	BX-0752 @ 30ft
Side (psi)	22.8	16.2	8.4
Roof (psi)	20.5	16.7	11.9

displacement curves would be very sensitive to any noise or errors in the acceleration data, since they would be magnified by the integration process.

UTK attempted to correct the integration errors by passing all the acceleration readings through low and high pass filters in order to remove the noise. However, as the type of accelerometer used for the blast test is unknown at this point, the manufacturer recommendations for descaling factors and removal of noise are unknown as well, which would lower the effectiveness of the band filtering process to some extent.

After the filtering process, the acceleration data for both BX-0751 and BX-0752 were improved with the removal of extreme peaks in acceleration. However, little improvement was observed in the filtered velocity and deflection curves past the 30msec measurement. For the BX-0751 data the filtered velocity curve returned to zero and the deflection curve leveled off near 50msec. However, no permanent deflection was observed after the actual blast test, which indicates that the filtered permanent deflection is not realistic. Similar problems occurred in the filtered data for BX-0752.

In addition, the type of accelerometer used in the blast test was designed for recording fast, high impact loads. Resolution of the accelerometer would not be high enough to precisely record the acceleration data after the peak pressure time. It is thus recommended by UTK that 1) only the positive and negative pressure phases of the blast, from 0 to 30msec, should be considered for determining maximum and minimum values of the acceleration, velocity, and displacement; 2) the maximum velocity and displacement values should be used with caution as the validity of the data could not be totally verified at this point due to lack of information.

The SDOF results closely estimated the deflection of the front wall but greatly

overestimated the velocity and acceleration. On the other hand, the Newmark-β analysis underestimated the deflections and velocities by half and provided accelerations that were much too small and not comparable to the experimental values. For both methods, the theoretical deflection values were the closest to the experimental results, with the velocity being the next best and the acceleration predictions the worst. This indicates that SDOF was a good prediction of the maximum deflection, but not of the subsequent velocity and acceleration. Thus only the deflection value from the SDOF analysis should be considered a valid theoretical value. For the Newmark-β analysis, the deflection and velocity, while unconservative, were comparable to the experimental results and may be used as a lower bound. However, the acceleration was a gross underestimate of the experimental acceleration and should not be used as a theoretical value.

4.5 Impulsive Blast Load

The maximum positive load duration of 4.3msec was experienced by the cubicle 30 ft from the blast. Given the sectional properties, the frequency for the front wall was calculated as 30Hz, which is close to 24 Hz, the natural frequency of the cubicle acquired from accelerometer readings. According to TM 5-1300 (1990) the blast load is impulsive if it is less than 25 percent of the fundamental period. A conservative estimate using the 30Hz natural frequency and 4.3msec blast duration found the blast load to be 12.9 percent of the fundamental period. Thus the loading caused by the blast was dependent on the impulse experienced during the pressure time loading.

The frequency was multiplied by the experimental positive phase impulse to obtain the force from the blast. A hand-calculation was conducted to determine the maximum

Table 4-7 Stress from blast impulse load

Cubicle	Impulse (psi-msec)	Max. Wall Tensile Stress $f_{bot,}$ (ksi)	Max. Wall Comp Stress f_{top} (ksi)	Yield Stress F_y (ksi)	Increase Factor IF	Dynamic Yield Stress F_{dy} (ksi)
BX-0751 @20ft	73.5	58.2	78.6	40	1.33	53.2
BX-0752 @25ft	68.6	54.4	73.5	40	1.33	53.2
BX-0753 @30ft	50.1	39.7	53.6	40	1.33	53.2

stresses in the front wall under the blast load, with the wall simplified as a simply-supported beam. The calculation results are summarized in Table 4-7 and full calculations included in the Appendix.

The design manual TM 5-1300 recommends using a yield stress of 40 ksi for cold formed steel unless the actual yield stress is known. The steel panels used in the blast cubicles had a listed yield stress of 30-50 ksi, therefore, the TM 5-1300 recommended value of 40 ksi was used in the analysis. TM 5-1300 increases the strength of the steel with a strength increase factor of 1.21 and a dynamic increase factor (DIF) of 1.1 for a total yield stress increase of $1.33*F_y$.

In the theoretical analysis, the blast load resulted in the yielding of cubicles BX-0751 and BX-0752, which could be a conservative under-estimate of the structural strength, as both cubicles showed no obvious signs of yielding and inelastic deformation after the blast test. Several factors could contribute to this under-estimating:

1) The yield stress range was from 30-50 ksi, which means the steel may have a yield stress up to 50 ksi. The assumption of the 40 ksi yield strength could be conservative without further information on the actual material yield stress from a coupon test.

2) Damping and partially fixed connections were not considered in the calculation. Although a small effect, damping slightly reduces the load experienced by the cubicle. On the other hand, partially fixed connections would increase stiffness, increasing natural frequency and hence increasing the load.

3) The wall was idealized as a beam when it is actually a plate with partially fixed connections on all four sides. Thus the edges would not be free to rotate and the stress redistributed throughout the plate offering additional capacity.

4) The calculated natural frequency of 30Hz was conservative given the measured frequency was 24Hz. The lower natural frequency results in a 20% lower experienced load.

Given the conservative assumptions in the calculation of the yield stress and other stated factors, it is proposed that the BX-0751 blast cubicle was likely close to its limit. The structural design of the blast cubicle is efficient and economical without waste of material.

4.6 Summary and Conclusions

Based on the test observations and data analysis, the following summary and conclusions were made:

1. Maximum positive blast pressure on the front wall increases exponentially as the stand-off distance decreases.
2. Positive impulse on the front wall increases as the stand-off distance decreases, but not as drastically as maximum positive pressure.
3. Maximum positive blast pressure and positive impulse on the side wall increases

as the stand-off distance decreases.

4. The cubicles exhibit elastic behavior during the blast test with no inelastic deformation observed after the blast test, except the roofs, which buckled upward due to the negative blast pressure. An addition of steel panels to the roof would likely increase the stiffness and prevent extreme deformations.
5. Acceleration, velocity, and deflection values are only considered valid from 0 to 30msec and should be used with caution.
6. The SDOF analysis provides close estimates for deflection and overly conservative values for velocity and deflection. Newmark-β method is not recommended for the prediction of deflection, velocity, and acceleration.
7. BX-0751 blast cubicle was likely close to its limit. The structural design of the blast cubicle is sufficient and economical without waste of material.

Chapter 5: Recommendations and Future Work

The manual *Structures to Resist the Effects of Accidental Explosions, Army TM 5-1300* was used to predict the pressure loading on steel blast cubicles and validate the experimental results. Based on the test results and analysis, TM 5-1300 was, while not perfect, conservative in prediction of blast loads. Further research into the behavior of blast waves and their interaction with structures would likely increase the accuracy of this design method. While beyond the scope of this thesis, a finite element analysis of the cubicles would provide an improved understanding of the structural behavior and response to blast loads.

There are many design manuals available for structural design to resist blast effects but the most widely used is TM 5-1300 (1990). One reason for its widespread use is its approval for public release with unlimited distribution. Until recently, most blast research has been performed by military or government organizations with their design manuals becoming the standard reference for civilian engineers. While the ASCE publications provide guidance for blast design they are not design manuals. Thus, a design code used either in conjunction with or independently of TM 5-1300 (1990) and similar manuals is needed for applications to structural design for civilian applications.

The design manuals employed in this thesis only employ SDOF systems for calculating the dynamic structural response. While approximate, SDOF calculations generally provide good accuracy in support of design. However, a closer approximation may be made through the use of finite element programs that analyze the non-linear response of the structure. While providing accurate prediction of behavior from blast

loads the finite element analysis requires some expertise. Therefore, for the designer new to blast design, the use of SDOF manuals and programs may be the simpler and less time consuming option.

There is an immediate need for experimental research into the behavior of structural steel to blast loads. While numerous numerical studies have been performed, the true behavior of steel structures exposed to blast cannot be determined without experimental testing. The critical areas of research are connections, splice plates, base plates exposed to localized blasts, and the overall behavior of steel frames exposed to stand-off blast loads.

References

References

ASCE. (1985). “Design of Structures to Resist Nuclear Weapon Effects.” Manual No. 42. American Society of Civil Engineers, New York, NY.

ASCE. (1999). “Structural Design for Physical Security: State of the Practice,” American Society of Civil Engineers, Reston, VA.

Baker, W.E. (1973). “Explosions in Air.” University of Texas Press, Austin.

Baker, W.E., Cox, P.A., Westine, P.S., Kulesz, J.J., and Strehlow, R.A. (1983). “Explosion Hazards and Evaluation.” Elsevier Scientific Publishing Company, New York.

Biggs, J.M. (1964). “Introduction to Structural Dynamics.” McGraw-Hill, Inc. New York, New York.

Bogosian, D., Ferritto, J. and Shi, Y. (2002). “Measuring uncertainty and conservatism in simplified blast models.” 30th Explosives Safety Seminar, Atlanta, GA.

Brode, H.L. (1955). “Numerical Solutions of Spherical Blast Waves.” Journal of Applied Physics. 26 (6), 766-775.

Chock, J., and Kapania, R. (2001). “Review of two methods for calculating explosive air blast.” The Shock and Vibration Digest. 33(2), 91-102.

Crawford, J., and Liu, C. (2006). “Minimization of Blast Effects Damage on Critical Buildings.” Global Security Asia Conference, Singapore.

DOE/TIC-11268. (1992). “A Manual for the Prediction of Blast and Fragment Loadings on Structures.” U.S. Department of Energy, Washington, D.C.

Dusenberry, D.O. (2003). “General Considerations for Blast-resistant Design of Facilities.” Engineering Smarter Proceedings of the 2003 structures congress and exposition.

Ettouney, M., Smilowitz, R., Rittenhouse, T. (1996). “Blast Resistant Design of Commercial Buildings.” Practice Periodical on Structural Design and Construction, February. 1(1), 31-39.

Glasstone, S. and Dolan, P.J. (1977). “The Effects of Nuclear Weapons 3rd Edition.” United States Dept. of Defense and the Energy Research and Development Administration.

Jacinto, A.C., Ambrosini, R.D., and Danesi, R.F. (2001). "Experimental and computational analysis of plates under air blast loading." International Journal of Impact Engineering. 25, 927-947.

Kingery, C.N. and Bulmash, G. (1984). "Technical Report ARBRL-TR-02555: Air Blast Parameters from TNT Spherical Air Burst and Hemispherical Surface Burst." U.S. Army Ballistic Research Laboratory, Aberdeen Proving Ground, MD.

Krauthammer, T., and Oh, G.J. (1998). "Blast-resistant structural steel connections." Structures under shock and impact. 5, 63-72.

Lawver, D., Daddazio, R., Vaughan, D., Stanley, M., and Levine, H. (2003). "Response of AISC Steel Column Sections to Blast Loading." Problems Involving Thermal-hydraulics, Liquid Sloshing, and Extreme Loads on Structures. PVP 454, 139-148.

Longinow, A. and Alfawakhiri, F. (2003). "Blast Resistant Design with Structural Steel Common Questions Answered." Modern Steel Construction. 43(10), 61-66.

Lu, Binggeng, and Silva, Pedro F. (2006). "Estimating equivalent viscous damping ratio for RC members under seismic blast loadings." Mechanics Research Communications. 33, 787-795.

Marchand, K.A., Alfawakhiri, F. (2004). "Facts for Steel Buildings - Blast and Progressive Collapse." American Institute of Steel Construction.

Mays, G.C., and Smith, P.D. (1995). "Blast Effects on Buildings." Thomas Telford Services Ltd., London.

Mills, C.A. (1987). "The Design of Concrete Structures to Resist Explosions and Weapon Effects." 1st International Conference on Concrete for Hazard Protection, Edinburgh, 61-73.

Newmark, N.M. (1972). "External Blast." Proceedings of the International Conference on the Planning and Design of Tall Buildings. Lehigh University, Vol. Ib, 661-676.

Ngo, T., Mendis, P., Gupta, A. and Ramsay, J. (2007). "Blast loading and blast effects on structures – an overview." Electronic Journal of Structural Engineering Special Issue: Loading on Structures.

Nonoka, T. (2000). "Shear failure of a steel member due to a blast." International Journal of Impact Engineering. 24(3), 231-238.

Sabuwala, T., Linzell, D., and Krauthammer, T. (2005). "Finite element analysis of steel beam to column connections subjected to blast loads." International Journal of Impact

Engineering. Volume 31(Issue 7), 861-876.

Smith, P.D. and Hetherington, J.G. (1994) “Blast and Ballistic Loading of Structures.” Butterworth-Heinemann, Oxford.

Sparling, B.F., Khosravani, R., and Neis, V.V. (1997). “The Dynamic Response of a Steel Building to Blast Loading.” Annual Conference of the Canadian Society for Civil Engineering. 4, 21-30.

Sunshine, D., Amini, A., Swanson, M. (2004) “Overview of Simplified Methods and Research for Blast Analysis.” Building on the past, securing the future proceedings of the 2004 structures conference. 1479-1489.

TM 5-1300. (1990).“Structures to resist the effect of accidental explosions.” U.S. Department of the Army, Navy, and Air Force Technical Manual.

TM 5-855-1. (1986). “Fundamentals of Protective Design for Conventional Weapons.” U.S. Department of the Army, Washington, D.C.

Urgessa, G. and Maji, A. (2006). “Blast Response of Carbon-fiber Reinforced Masonry Walls.” Proceedings of the 2006 SEM Annual Conference and Exposition on Experimental and Applied Mechanics. 3, 1682-1690.

Zain, Mohammed. (2006). “Finite element analysis of storm shelters subjected to blast loads.” Doctoral dissertation, Department of Civil Engineering, Texas Tech University, Lubbock, TX.

Appendix

Composite Section Properties (for determining stiffness)

Channel (from James Waller calc. on 1/23/01 - Comp. sys. w/ cond)

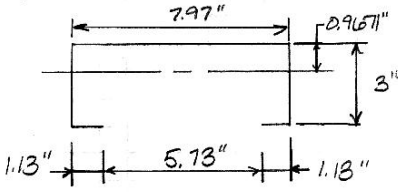

$I = 1.0937 in^4$

$\bar{y}_{top} = 0.9671"$

$A = 0.8131 in^2$

$$W_{channel} = 0.8131 in^2 \left(\frac{490 lb/ft^3}{1728 in^3/ft^3}\right) = 0.2306 lb/in = 2.767 lb/ft$$

Composite Wall (analyze as simply supported beam)

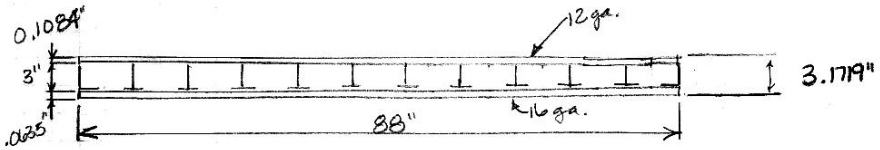

Find neutral axis

$$Q_1 = .8131 in^2 (.9671" + .1084") 11 + .0635" (88") (3.1719 - \tfrac{.0635}{2}) + .1084" (88") (.1084/2)$$

$$Q_1 = 9.619 + 17.55 + 0.517 = 27.69 in^3$$

$$A_1 = .8131 in^2 (11) + .0635" (88") + .1084" (88") = 24.07 in^2$$

$$\bar{y}_{top,1} = Q/A = \underline{1.15"}$$

Find I for comp. section

$$I_{comp1} = \frac{88 (.0635)^3}{12} + .0635 (88) (3.1719 - .0635/2 - 1.15)^2 + 1.0937 in^4 (11)$$

$$+ 0.8131 in^2 (.1084 + 0.9671 - 1.15)^2 (11) + \frac{88" (.1084)^3}{12} + 88 (.1084 in) (1.15 - .1084/2)^2$$

$$I_{comp1} = .0019 + 22.13 + 12.081 + .6996 + .0093 + 11.45$$

$$I_{comp1} = \underline{45.67 in^4}$$

Determine mass of wall

Sand

$\rho = 109\ lb/ft^3$

$A_{sand} = 3"(88") - 11(.813in^2) = 255.06\ in^2$

$w_{sand} = 109 lb/ft^3\ (255.06in^2)\left(\frac{1ft^2}{144in^2}\right)$

$w_{sand} = 193.1\ lb/ft$

12 ga outside panel

$w = .1084"(88")\ 490\ lb/ft^3\left(\frac{1ft^2}{144in^2}\right) = 32.46\ lb/ft$

16 ga inside panel

$w = .0635"(88")490\left(\frac{1}{144}\right) = 19.015\ lb/ft$

$w_{tot} = 193.1 + 32.46 + 19.015 + 2.767(11) = 275.01\ lb/ft = 22.92\ lb/in$

$m_{wall} = \frac{22.92\ lb/in}{386.4\ in/s^2}$

$m_{wall} = .0593\ \frac{lbs^2}{in^2}$

Find frequency of wall

$\omega_n = \frac{\pi^2}{L^2}\sqrt{\frac{EI}{m}} = \frac{\pi^2}{(88")^2}\sqrt{\frac{29000000psi\ (45.67in^4)}{.0593\ lbs^2/in^2}}$

$\omega_n = 190.17\ rad/s$

Composite Section properties (for wall capacity & stress)

*Ignore the flexural capacity of the 12ga. blast panel

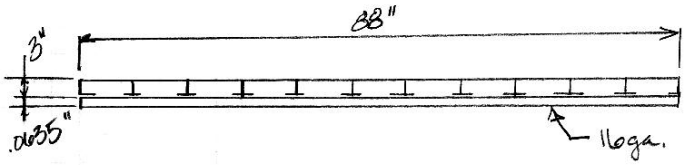

Find neutral axis

$Q_{\bar{z}} = .8131in^2\,(.9671")(11) + .0635"(88")(3.0635 - \frac{.0635}{2})$

$Q_{\bar{z}} = 8.6498in^3 + 16.94in^3$

$Q_{\bar{z}} = 25.59in^3$

$A_{\bar{z}} = .8131in^2(11) + .0635"(88")$

$A_{\bar{z}} = 14.53in^2$

$\bar{y}_{top\bar{z}} = Q/A = 1.76"$

Find I for comp. section

$I_{comp\bar{z}} = \frac{88"(.0635")^3}{12} + .0635(88)(3.0635 - \frac{.0635}{2} - 1.76)^2$

$+ 1.0937in^4(11) + .8131in^2(.9671 - 1.76)^2(11)$

$I_{comp\bar{z}} = .00188 + 9.038 + 12.031 + 5.62$

$I_{comp\bar{z}} = 26.69in^4$

$S_{b\bar{z}} = \frac{I}{c_b} = \frac{26.69in^4}{3.0635 - 1.76}$ $\qquad$ $S_{t\bar{z}} = \frac{I}{c_t} = \frac{26.69in^4}{1.76}$

$S_{b\bar{z}} = 20.48in^3$ $\qquad$ $S_{t\bar{z}} = 15.16in^3$

Find stress from blast load

Analyze as simply supported beam

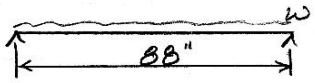

BX-0751

$i_r^+ = 73.5$ psi-ms

$F_o = \omega_n \text{ Area} = \omega_n i_r^+$

$F_o = 190.47 \text{ rad/s} \; (73.5 \text{ psi-ms}) \left(\frac{s}{1000 \text{ ms}}\right)$

$F_o = 13.99$ psi

$\omega = 13.99 \text{ psi} \; (88") \; (12"/\text{ft})$

$\omega = 14.77 \text{ k/l}$

$M_u = \frac{\omega l^2}{8} = \frac{14.77 \text{ k/l} \; (88/12')^2}{8}$

$M_u = 99.28 \text{ k-l}$

$f_b = \frac{M_u}{S_{b2}} = \frac{99.28 \text{ k-l}}{20.48 \text{ in}^3} \; (12"/\text{l})$

$f_{btm} = 58.2$ ksi

$f_{top} = \frac{M_u}{S_{t2}} = \frac{99.28 \text{ k-l} \; (12"/\text{l})}{15.16 \text{ in}^3}$

$f_{top} = 78.6$ ksi

BX-0152

$i_r^+ = 68.6$ psi-ms

$F_o = 190.47 \text{ rad/s}\,(68.6 \text{ psi-ms})\left(\frac{s}{1000 \text{ ms}}\right)$

$F_o = 13.07$ psi

$\omega = 13.07 \text{ psi}\,(88'')(12''/1')$

$\omega = 13.8 \text{ k/l}$

$M_u = \frac{13.8 \text{ k/l}\,(88/12)^2}{8} = 92.8 \text{ k}$

$f_b = M_u / S_{b2} = 92.8^{k}/_{20.48 \text{ in}^3}(12)$

$f_{btm} = 54.9$ ksi

$f_{top} = \frac{M_u}{S_{t2}} = \frac{92.8^{k}(12)}{15.16 \text{ in}^3}$

$f_{top} = 73.5$ ksi

BX-0753

$i_r^+ = 50.1$ psi-ms

$F_o = 190.47 \text{ rad/s}\,(50.1 \text{ psi-ms})$

$F_o = 9.54$ psi

$\omega = 9.54 \text{ psi}\,(88'')\,(12)$

$\omega = 10.07 \text{ k/l}$

$M_u = \frac{10.07 \text{ k/l}\,(88/12)^2}{8}$

$M_u = 67.7 \text{ k}$

$f_b = \frac{M_u}{S_{b2}} = \frac{67.7^{k}\,(12''/1')}{20.48 \text{ in}^3}$

$f_{btm} = 39.7$ ksi

$f_{top} = \frac{M_u}{S_{t2}} = \frac{67.7^{k}\,(12''/1')}{15.16 \text{ in}^3}$

$f_{top} = 53.6$ ksi

$F_b = 1.33\ F_{ya}$ (TM 5-1300, Eq 5-26)

TM 5-1300 includes a dynamic increase factor of 1.33,

$F_b = 1.33(40\ ksi)$

$F_b = \underline{53.2}\ ksi$

Vita

Sarah Beth Janney was born in Latrobe, PA, on May 11, 1983. She was raised in Knoxville, TN, where she attended the Farragut schools and graduated in 2001. She received a B.S. in civil engineering in May, 2006, and an M.S. in civil engineering in December, 2007, from the University of Tennessee, Knoxville.